EXPERIMENTAL INVESTIGATION OF RATES AND MECHANISMS OF ISOTOPE EXCHANGE (O,H) BETWEEN VOLCANIC ASH AND ISOTOPICALLY-LABELED WATER

by

GARY S. NOLAN

A THESIS

Presented to the Department of Geological Sciences
and the Graduate School of the University of Oregon
in partial fulfillment of the requirements
for the degree of
Master of Science

March 2012

THESIS APPROVAL PAGE

Student: Gary S. Nolan

Title: Experimental Investigation of Rates and Mechanisms of Isotope Exchange (O,H) between Volcanic Ash and Isotopically-Labeled Water

This thesis has been accepted and approved in partial fulfillment of the requirements for the Master of Science degree in the Department of Geological Sciences by:

Ilya Bindeman	Chairperson
Mark Reed	Member
Paul Wallace	Member

and

Kimberly Andrews Espy	Vice President for Research & Innovation/Dean of the Graduate School

Original approval signatures are on file with the University of Oregon Graduate School.

Degree awarded March 2012

THESIS ABSTRACT

Gary S. Nolan

Master of Science

Department of Geological Sciences

March 2012

Title: Experimental Investigation of Rates and Mechanisms of Isotope Exchange (O,H) between Volcanic Ash and Isotopically-Labeled Water

The hydrogen and oxygen isotope ratios in hydrous minerals and volcanic glass are used as paleo-proxies to infer isotopic values of meteoric waters and thus paleo-climate conditions. Long-term exposure experiments with Mt Mazama ash reacted with isotopically labeled water (+650‰ $\delta^{2}H$, +56‰ $\delta^{18}O$) at 70, 40 and 20°C show $\delta^{2}H$ increase with time and faster deuterium uptake at higher temperatures. Times ranged in duration from 24 to 14454h. Long duration exposure shows no net increase in water nor $\delta^{18}O$ in ash. Ash was analyzed by TC/EA mass spectroscopy, thermogravimetric analysis and infrared spectroscopy (KBr pellets) measuring $\delta^{2}H$, total water, and OH water peaks. This study demonstrates $\delta^{2}H$ in ash changes by minor diagenesis even at relatively low temperatures of 20°C. A diagenetic history of ash is needed to interpret $\delta^{2}H$, but $\delta^{18}O$ values are more robust.

This thesis includes both previously unpublished and co-authored material.

CURRICULUM VITAE

NAME OF AUTHOR: Gary S. Nolan

GRADUATE AND UNDERGRADUATE SCHOOLS ATTENDED:

University of Oregon, Eugene, Oregon
Oregon State University, Corvallis, Oregon
Northern Arizona University, Flagstaff, Arizona

DEGREES AWARDED:

Master of Science, Geological Sciences, 2012, University of Oregon
Master of Science, Chemistry, 1979, Oregon State University
Bachelor of Science, Chemistry, 1976, Northern Arizona University

AREAS OF SPECIAL INTEREST:

Isotope geochemistry
Natural products and phytochemistry

PROFESSIONAL EXPERIENCE:

Science lab manager, Chemist, University of Oregon & Oregon State 26 years

Project Manager, East Earth Herb 2 years

GRANTS, AWARDS, AND HONORS:

Sigma Xi Research, X-ray diffraction, Northern Arizona University, 1975-76

Magna cum Laude, Northern Arizona University, 1976

PUBLICATIONS:

He X.G., Bernart M.W., Nolan G.S., Lin, L.Z. and Lindenmaier M.P. (2000) High-Performance Liquid Chromatography-Electrospray Ionization-Mass Spectrometry Study of Ginkgolic Acid in the Leaves and Fruits of the Ginkgo Tree (Ginkgo Biloba). *Journal of Chromatographic Science* **38** (4) 169–173.

Lin L.Z., He X.G. Lindenmaier M. and Nolan G. (2000) Liquid Chromatography-electrospray Ionization Mass Spectrometry Study of the Flavonoids of the Roots of Astragalus Mongholicus and A. Membranaceus *Journal of Chromatography A*. **876**, (1–2) 87-95

Siggel M. R. F., Nolan G.S., Saethre L.J., Thomas T.D. and Ungier, L. (1987) Electron donating ability of ethyl and ethenyl groups from core electron spectroscopic and ab initio theory. A study of CH_3CH_2X and CH_2CHX (X= F, Cl, Br, I) Journal *of Physical Chemistry* **91**(15) 3969-74

Nolan G.S., Saethre L.J., Siggel M.R., Thomas, T.D., and Ungier L. (1985) Electron-donating ability of aliphatic and aromatic rings. *Journal of the American Chemical Society* , **107**(23) 6463-7

Aitken E.J., Bahl M.K., Bomben K.D., Gimzewski J.K., Nolan G.S. and Thomas, T.D. (1980) Electron spectroscopic investigations of the influence of initial and final state effects on electronegativity. *Journal of the American Chemical Society*, **102**(15) 4873-9

Nolan G. S., Gleicher G. J., Schatz B.S., and Cordova R (1980) Substituent effects in hydrogen abstraction from 10-substituted-9-methyl anthracenes. Correspondence with ring substitution. *Journal of Organic Chemistry* **45**(3) 444-7

ACKNOWLEDGMENTS

I would like to thank Jim Palandri for help in the lab, Paul Wallace for advice on FTIR, Dr Martin Weisner for providing size distribution of ash sample, Ben Ellis for XRF analysis of ash, Tim Howe for ^{2}H and ^{18}O analysis of water, NSF grant EAR-0805872 for funding.

This work is dedicated to my life partner Laura whose patience has contributed immeasurably to the completion of this project.

TABLE OF CONTENTS

Chapter Page

LIST OF FIGURES

LIST OF TABLES

Table Page

CHAPTER I

INTRODUCTION

Co-authored and unpublished material (with Ilya Bindeman) is presented in the Introduction, Methods, Results, and Discussion chapters. Experimental work was performed by me. The writing is entirely mine. I. Bindeman provided editorial assistance.

The isotopic composition of water is determined by factors such as distillation, condensation, temperatures and humidity (e.g. Gat, 2010) . Well-understood correlations of $\delta^{18}O$ vs temparature, latitudes and elevation for modern world (Dansgaard, 1964; Rowley et al., 2001) permit uniformitarian application of these isotopic ratios to paleoenvironments. Given that ^{2}H and ^{18}O isotopes are incorporated into secondary minerals or glass during weathering and hydration it is not surprising that the hydrogen and oxygen isotopic aqueous signatures of hydrous surface materials have been the focus of studies of paleoclimate (Friedman et al., 1992; Friedman et al., 1985; Friedman et al., 1992) as well as ancient topography (Chamberlain & Poage, 2000). These include the ^{2}H in kaolinite (Mulch 2006), and ^{18}O in clay minerals (Chamberlain & Poage, 2000), as well as goethite (Bao et al., 2000), phosphate, and many other minerals. A critical assumption in these paleo-isotope works is the stability of the chemical form of the originally incorporated isotope. Volcanic ash has a particular value for both ^{18}O and ^{2}H isotopes (Friedman et al., 1992; Friedman et al., 1993) because the ash is produced and spread over climatically diverse territories instantaneously. As ash hydrates without alteration within a few hundreds years upon deposition (Friedman et al., 1993), a shallowly buried blanket of ash potentially records isotopic values of enviromental water, providing a snapshot view of precipitation across continents or mountain ranges.

However, there has not been an experimental demonstration of stability of the isotopic record in ash. In particular, while reasonable mechanistic arguments can be made for the chemical stability of incorporated ^{18}O (e.g. Friedman et al., 1993), the same needs to be tested for hydrogen (deuterium), well known for its proclivity to exchange rapidly. In particular, it is assumed that within several thousand years of weathering and exposure to environmental waters of a particular isotopic value, water in-diffusion hydrates the ash (or clay) to its full capacity of around 4 wt% water. This process yields a weathering-time averaged meteoric and hence climate snapshot during the period of reaction (Friedman et al., 1993). A critical assumption is that upon full hydration the secondary water does not exchange isotopically with changing environmental waters, and thus these thousand-year scale averages of isotopic signal can be trusted in old ashes.

Anovitz et al. (2009a) tested the general stability of the hydrous portion of ash by exposing obsidian to alternate sequences of water and pure deuterium oxide at high temperature. Concluding that overprinting occurs with the new solvent front, they also note the apparent alteration of "intrinsic" water in the obsidian. This work is in addition to several low temperature diffusion studies employing SIMS (Anovitz et al., 2004; Anovitz et al., 2008; Riciputi 2002) providing useful perspectives on environmental fates of glasses as well as diffusion data.

Our experiments explore and investigate the volcanic ash itself, the ability of volcanic ash to exhange with environmental waters, including water uptake, deuterium exchange and oxygen exchange. These long term experiments (up to 14450 hours) at 20°,

40°, and 70°C test the ability of ash to retain or record the changes of water concentrations and water isotopes in near-surface to shallow diagenetic environments.

CHAPTER II

METHODS

Co-authored and unpublished material is presented in this chapter. Aside from outside lab work on particle size, water analysis, and elemental analysis (listed in acknowledgements) all experimental work was performed by me as was the development and optimization of IR technique. The writing is entirely mine. I. Bindeman provided editorial assistance.

2.1. Starting ash material and water

The 7600 ka Mt Mazama ash (Table 1, starting chemical composition) was collected at the Hells Canyon landing station of Idaho (46°05'23.85" N 116° 59' 04.4" and 267m elevation) Heller Bar Boat launch Idaho/Washington State boundary on the bank of the Snake River. Microscopic examination of the ash reveals that nearly all particles are less than 0.1 mm , as also determined by laser (fig. 1) by laser light scattering. Ash material is opaque under cross polars with much less than .1% evincing birefringence, suggesting that it is at least 99% fresh glass with few phenocrysts or detrital grains. This uniformity is borne out by SEM analysis as well (figure 3 a-c).

A chemical analysis of the ash (Table 1) recalculated into a basic SiO_2 framework yields the following chemical "formula": $Ca_{0.04}Na_{0.11}K_{0.04}Mg_{0.01}Fe_{0.02}Al_{0.19}Si_{0.78}O_2$, suggesting that the ash is mostly Na-K Alumino-silica glass. The sum of group I and II cation charges balances the negative charge of tetra-substituted framework Al. Thus it is likely group I and II cations are not network oxides.

Table 1. Elemental analysis of starting material by XRF.

Normalized Major Elements	**Weight %**	**Trace Elements**	**ppm**	**CIPW Normalization**	
SiO_2	70.63	NiO	5.3	Normative Mineral	Weight % Norm
TiO_2	0.484	Cr_2O_3	8.5	Quartz	24.25
Al_2O_3	14.87	Sc_2O_3	10.6	Plagioclase	52.04
FeO*	2.51	V_2O_3	52.7	Orthoclase	16.24
MnO	0.058	BaO	809.0	Diopside	3.11
MgO	0.76	Rb_2O	54.6	Hypersthene	1.99
CaO	2.98	SrO	398.4	total	97.63
Na_2O	4.93	ZrO_2	295.0		
K_2O	2.65	Y_2O_3	29.3		
P_2O_5	0.123	Nb_2O_5	7.9		
total	99.995	Ga_2O_3	21.5		
*All Fe as FeO		CuO	26.0		
		ZnO	59.9		
		PbO	12.2		
		La_2O_3	24.2		
		CeO_2	47.7		
		ThO_2	4.5		
		Nd_2O_3	22.7		
		U_2O_3	2.0		

Quantitative particle size and surface area data on a Mazama ash sample was measured by a Beckman Coulter LS 13 320, multi-wavelength particle size analyzer employing a laser light scattering technique. Data are provided in figure 1.

Both native and reacted ash were examined under an FEI Quanta 200 ESEM/VPSEM Microscope at the University of Oregon Camcor facility (fig. 3 a-f). This was done for two purposes: 1) to examine the morphology of ash particle and 2) to determine any morphological changes brought by the exposure to water after extended exposure to water. The general particle shape informs the understanding of surface area and estimating the surface/volume ratio of a hypothetical ash particle as compared to a sphere of similar volume. Formation of degradation products or clay minerals were not observed after extended immersion times.

The deuterium- and ^{18}O-enriched water was prepared by adding pure deuterium oxide, and 10% H218O Cambridge Isotope Labs lot number 7G-506, to water delivered to the distilled tap in Eugene Ore (determined to be -81.15‰ d^2H, -11.17‰ $\delta^{18}O$). Of the deuterium oxide, .5428 g. was diluted to around 5 l. as measured by a 6 l Erlenmeyer flask. This enriched water additionally received 6.831 g. 10% $H_2{}^{18}O$, Cambridge Isotope Labs lot number PR-16742. The prepared water was analyzed for δ^2H and $\delta^{18}O$ by H_2 and CO_2 equilibration techniques at the University of Alaska Fairbanks, and yielded +56.1 ‰ ($\delta^{18}O$) and +651‰ (d^2H) values.

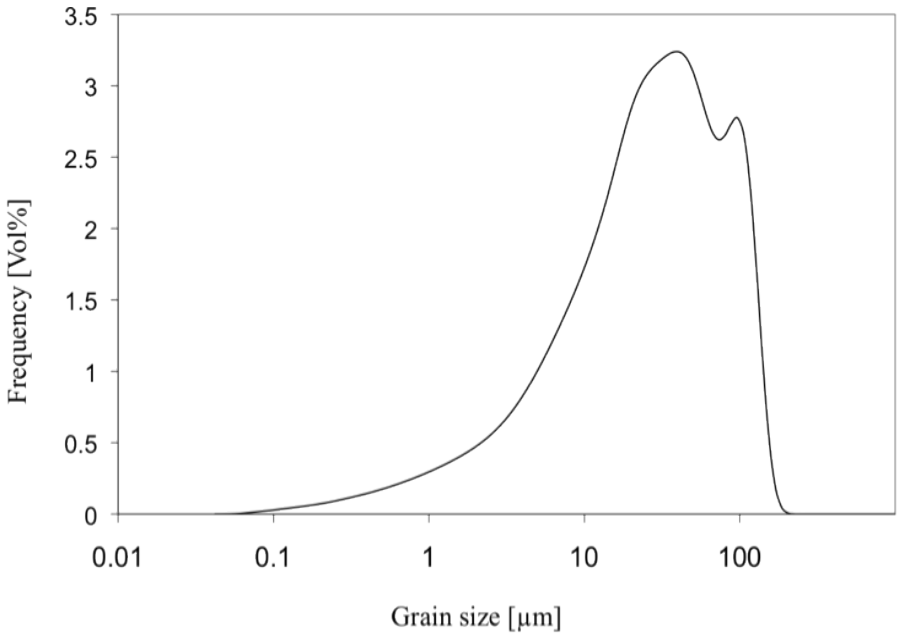

Figure 1

Figure 1. Mazama ash grain size distribution. Particle size variation for Mt. Mazama ash sample, collected about 537 km from the eruption site, Crater Lake, in southern Oregon. The skewing to smaller particles is consistent with stratospheric transport (e.g. Sarna-Wojcicki, et al 1981) and aerial sorting. The mean diameter of Mt. St. Helens ash at this distance was just under 50 µ (Sarna-Wojcicki, et al 1981). This analysis yielded a mean size of 39 µ, a median of 27, and a specific surface area (surface to volume ratio) of 10652 cm^{-1} or 1.065 $microns^{-1}$. Please see Appendix D for elaboration of this analysis.

2.2. Vacuum oven and muffle furnace experiments and TGA analysis

Setting a standard drying time and protocol was an important detail of this work which allows comparison of runs at different exposure times. Preliminary estimation of loss on dry was done with the native ash in a vacuum oven set at a temperature of 130 ºC. There is considerable variability in the amounts of water removed at all of the drying times (this variability was seen in all the TCEA results as well). In

general lab drying at 130 ºC decreased water content by around 1 to 1.2% water. Once this amount was removed, further weight loss was minimal upon further heating. After examination of time intervals of heating a time of 48 hours under vacuum at 130 ºC was set for all samples destined for TCEA/MS.

Drying to higher temperatures as part of step heating analyses and IR standard preparation was done in a digitally monitored muffle furnace. Starting at 25 ºC for the first sequence step, heated native ash samples were withdrawn at intervals of 100 ºC up to 900 ºC. A second analysis with two sets of samples was also performed. This involved concurrent step heating and sample removal: one of these was ash reacted for 7300 hours in deuterated water, the other a second round of native ash. Sampling was done at 25, 150, 200, 250, 300, 350, 400, 450, 600, 750 and 900 degrees C. All of these heat-processed samples were subject to TCEA/MS and infrared analyses were obtained on the (heated) native ashes only.

A more sensitive drying analysis was performed using thermogravimetric analysis or TGA. This was done on a TA Instruments Thermogravimetric Analyzer (TGA Q500). A run consisted of 12-18 mg. ash slowly thermally degassed (20 ºC/min) under a nitrogen atmosphere. The continual loss was recorded as percent of original weight versus temperature.

2.3. Exposure experiments with isotopically-labeled water

Hydration occurred in the deuterium enriched water with exposure for various lengths of time. Temperature was held at one of three values: 70, 40, and 20ºC. The samples consisted of 100 mg. of ash in 3 ml. of the prepared water. Samples (ash plus

water) were put in 10 ml GasBench exetainers with rubber air-tight screw on top and held in constant temperature (±0.1°C variations) inside of the GasBench thermal block.

A second set of exposure experiments were constructed with ash that was first vacuum dried for 60 hours at 130 ºC. Other than the ash amounts being 10 mg the reaction conditions were identical to above. The ash amount was decreased to check for possible full consumption of reactive ash sites (saturation) and to further assure no effective decrease in concentration of ^{2}H in the (reactant) water as the reaction proceeds. This latter point is potentially useful for constructing kinetic models. Durations and outcomes of all (ash plus water) experiments are summarized in Table 5 in Appendix A.

Removal of water was a reaction-terminating event. As removal of the overlying water by filtration being difficult, samples were spun in a centrifuge and the supernatant was poured off or removed with a pipet. This was followed by three separate short rinses with distilled “Eugene” water (to remove surface water absorbed on ash). Each rinse was accompanied by shaking of the mixture and centrifugation to settle the solids. Lastly the ash was mixed with a volatile organic solvent ollowed by centrifugation as with the water rinsing steps. Samples were then air dried in isolation before drying by vacuum heating for many hours (described above). Samples once dried were capped and stored in a dessicator.

2.4. Isotope analyses

The front end TC/EA (Thermal Conversion Elemental analyzer, or pyrolysis furnace) continuous flow and sampling system at the University of Oregon is coupled through a molecular sieve, size exclusion stationary phase chromatography column to a large radius MAT253 10 kV gas source isotope ratio mass spectrometer (IRMS).

Hydrogen isotope measurements generally consumed 1-3 mg of the ash although for water-poor samples the amount ranged up to 6 mg. These were performed in continuous flow mode using the TC/EA furnace with glassy carbon. Samples were loaded and purged with He carrier gas in an autosampler. We used three reference standards in each of the analytical sessions (NBS30 biotite, δ^2H = -66‰, Butte (MT) quartz monzonite biotite δ^2H = –161.8‰, and RUH2 muscovite, δ^2H = -98.2‰) spanning a range of 95‰ and with a few exceptions overlapping the ranges of the unknowns (see Table 2). We applied a three point calibration using offsets between measured and nominal δ^2H values for the mica standards during each analytical session.

The analysis for hydrous ^{18}O in native and two ^{2}H -enriched, reacted ashes was done with 1-2 mg of ash also using TCEA-MAT253 GSMS (see Table 2) and a CO only method. Measurements for all ash samples were offset by the ^{18}O value for the undried native ash, the latter defined as the zero reference point. The absolute value is less important than a relative difference between exposed and non-exposed ash. Native and exposed ashes were run both with and without vacuum drying.

Internal errors with repeated standard analysis in the same analytical session typically ranged in ±0.05-0.1wt% water and ±2-3‰ d^2H; the external errors related to analysis of ash after handling and drying are estimated to be larger. While we have not performed strict error propagation, the repeated analysis of ash from identical separate experiment with nominally identical preparation and subsequent analysis conditions return results within 0.2-0.3wt% H_2O and 5-8‰ d^2H.

2.5. Infrared (FTIR) analyses of KBr pellets

Infrared analysis of water in glass and applications in the geological sciences has a long and extensive history, including the studies of fluid and melt inclusions (Bartholomew & Butler 1980; Wakabayashi 1989; Newman et al., 1986; Metrich and Wallace, 2008). Determining water concentration in a small and irregular glass fragments or mica (e.g. kaolinite) requires fairly extensive sample preparation in the form of cutting and polishing as part of the process of obtaining reproducibly precise path lengths. The use of pelletizing samples in KBr glass has been practiced for more than 50 years (Romo 1956; Kirkland 1955; Sobkowiak 1995). All samples were a combination of ash (45%) mixed with potassium bromide (55%) pressed into a wafer. Samples analyzed by infrared generally followed the same initial handling. Infrared grade potassium bromide, Fisher Scientific lot number 871087, was vacuum dried at 130 ºC to remove water. We used infrared grade potassium bromide and after vacuum drying obtained an absorption spectrum blank to ascertain whether there were contaminant absorbances (figure 8) in wavelength window of interest.

Sample homogenization was accomplished by extensive grinding of the ash and KBr in an agate mortar and pestle. This mixture was pressed into a 7 mm die with a hand press (Aldrich Quick Press pellet kit p/n Z506761). The pellet was cut from the die with a small razor knife and generally was recovered as a major fragment of the circle. Sample path length was determined with a digital micrometer and the value used was an average of at least eight separate measurements. Further details on FTIR procedure and measurements are provided in Appendix B.

The water concentration values were determined by infrared in KBr pellets using literature $\varepsilon_{3570} = 80 - (1.36 * C_{H2O})$, an iterative procedure (see below and Appendix B) that begins with an initial assumed ε_{3570}, (Leschik et al., 2004). These were compared with water measured by total extraction using TCEA and these values agreed reasonably well (see figure 10). Each of the native ash experimentally step-heated and isotopically analyzed ash samples had one infrared spectrum recorded for each temperature of sampling. Sample amounts were limited for the enriched water reacted sample and the native ash samples simultaneously taken at each sampling temperature were taken to be representative for both native and reacted ashes.

Through all of the above described methods a large collection of data was generated that bear on a description of the ash and reactions with the experimental water. This data set is the subject of the chapter that follows.

CHAPTER III

RESULTS

Co-authored and unpublished material is presented in this chapter. All data analysis was performed by me. The writing is entirely mine. I. Bindeman provided editorial assistance.

3.1. Thermogravimetric analysis results

The TGA heating analyses (fig. 7, and 8) results in stepwise removal of molecular and OH-bound water from ash and the pattern of weight loss is the same for the native ash and ash pre-dried in a vacuum oven at 130'C (fig. 8) The important observation from the TGA analysis, most relevant for this work, is that the rate of loss of water in the ash is minimal up to drying temperatures of around 200- 250°C, after which the slope greatly increases. This suggests that the vacuum drying protocols that we employed affect primarily the most loosely bound water. Perhaps even more important observation is that D/H ratio stays relatively constant during this drying. Above these temperatures, featureless, monotonic decline of weight (and residual water down to ~0.5wt%) at 600°C, followed by a more rapid collapse of the remaining ~0.5 wt % water to nearly 0% was observed.

3.2. SEM analysis

Figure 3 contains representative images of native and reacted ash. There is no visual indication of differences between the groups. We observed no secondary minerals in the reacted ash nor other degradation features down to 0.1 um resolution. As is evident from fine structures in comparisons there is no evidence of dissolution or diagenesis.

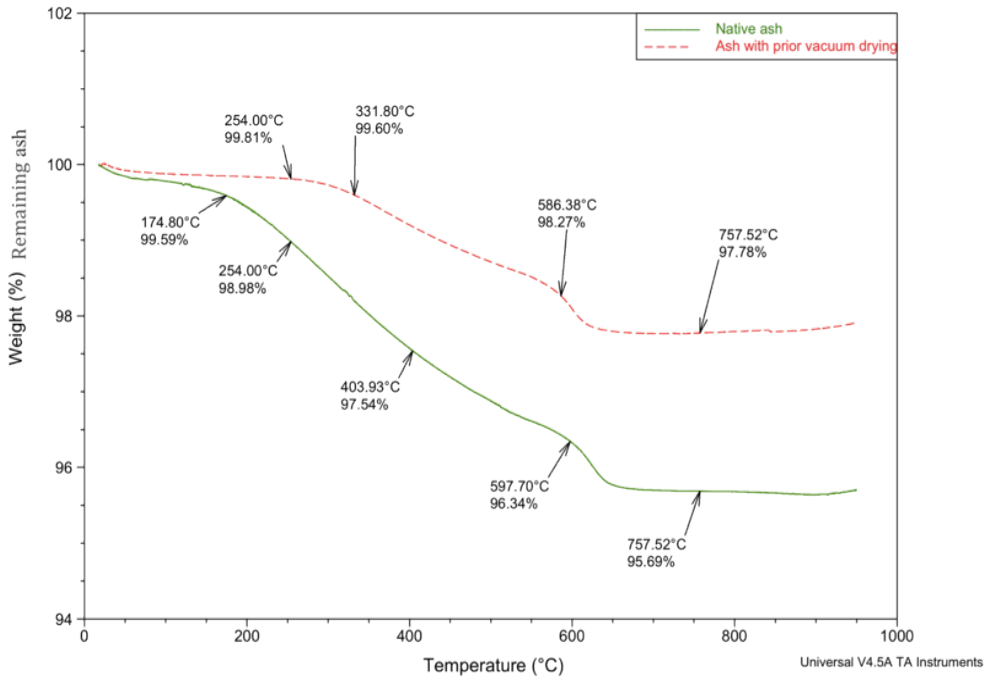

Figure 2

Figure 2. The TGA analysis of native ash and ash that was pre-dried in a vacuum oven for 60 h (~2.5 wt% water). Notice that both show roughly similar behavior upon drying, but for this pre-dried ash the onset of the higher rate of weight loss is delayed until over 250 °C

.

3.3. TC/EA Mass Spectroscopy Results

3.3.1. Deuterium TC/EA mass spectroscopy results

The most important result of our experiments is a linear increase in d^2H value in ash hydrated for progressively longer times, and no such trend for H_2O_{tot} and $\delta^{18}O$ water (see below). The rate of deuterium uptake in each of the isothermal time series measured from 48 to 14454 hours or roughly 602 days (~532 days for the 70 °C series) followed a generally linear trend (fig 4 a,b,c). Expectedly, there is increasing slope for each 20, 40 and 70°C time series experiments, and the rates of uptake are high: we are able to

measure higher d^2H values in a matter of few days at 70°C incubated ash. Results are tabulated in Table 2.

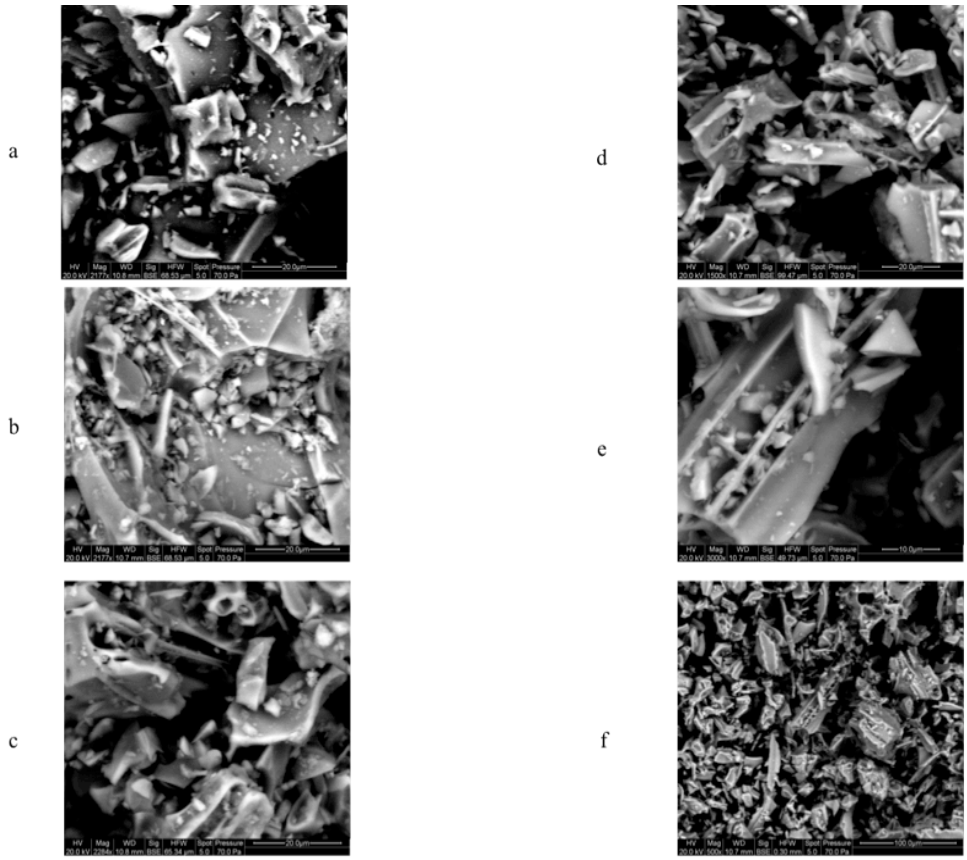

Figure 3

Figure 3 a-c. Native ash SEM images, d-f are those of ash reacted for 7017 hours. At this degree of SEM resolution it is clear the sharp ash ridges are preserved intact. Notice that there are no secondary clay minerals.

The rates of reaction for ash that was dehydrated prior to immersion measured from 25 to nearly 6000 hours or roughly 250 days (~57 days for the 70 °C series) followed a generally linear trend (Fig 5 a,b,c). Slopes for each 20, 40 and 70°C time series experiments successively increase with the rates of uptake much higher than seen

in (fig. 4 a,b,c). Each of the rates in figure (fig. 5 a,b,c) are highest at shorter reaction times with rates that moderate at longer periods. All rates at each temperature are much higher than the corresponding ones for the native (not dehydrated) ash (fig 4. a,b,c). Results are tabulated in Table 2.

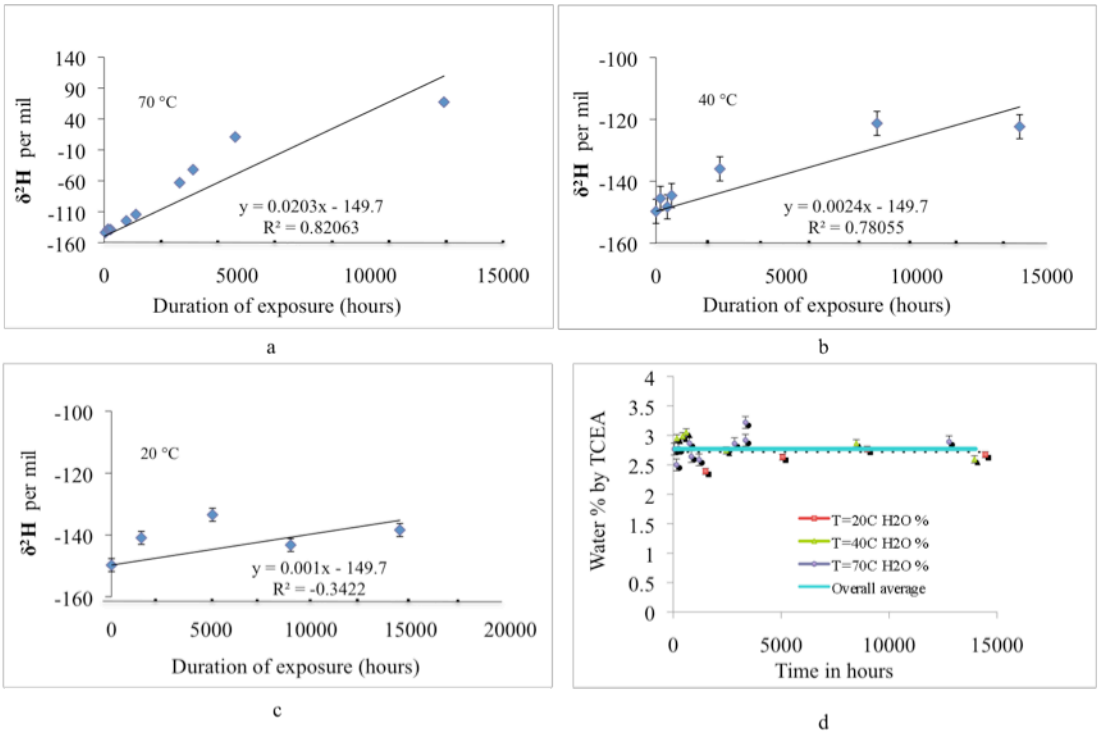

Figure 4

Figure 4 a-d. The δ^2H in initially undried native ash as a function of exposure time to isotopically-labeled water (+650‰ ∂^2H) a) at 70°C, b) at 40° C and c) and 20°C. Samples are all dried under vacuum at 125 °C for 48 hours after immersion period prior to analysis. Figure clearly indicates deuterium signal remains in the native ash after exposure to higher deuterium concentrations in surrounding water at 70 °C. Each data point represents averages of multiple trials with average standard deviations of 3.7 ‰ at 70 °C, 3.9 ‰ at 40 °C, and 2.1 ‰ at 20 °C with the error bars indicated at each data point. Linear regression fits are shown on the plots. Figure 4 d) shows the averages of water contents in the dried material as determined by TCEA, grouped by exposure temperatures, with uncertainties indicated with vertical error bars. Notice that the length of exposure to isotopically-labeled water does not increase water concentration. The water weight uncertainties exceed our analytical precision and are due to sample heterogeneities seen in the small sampling amounts. Data is summarized in Table 2.

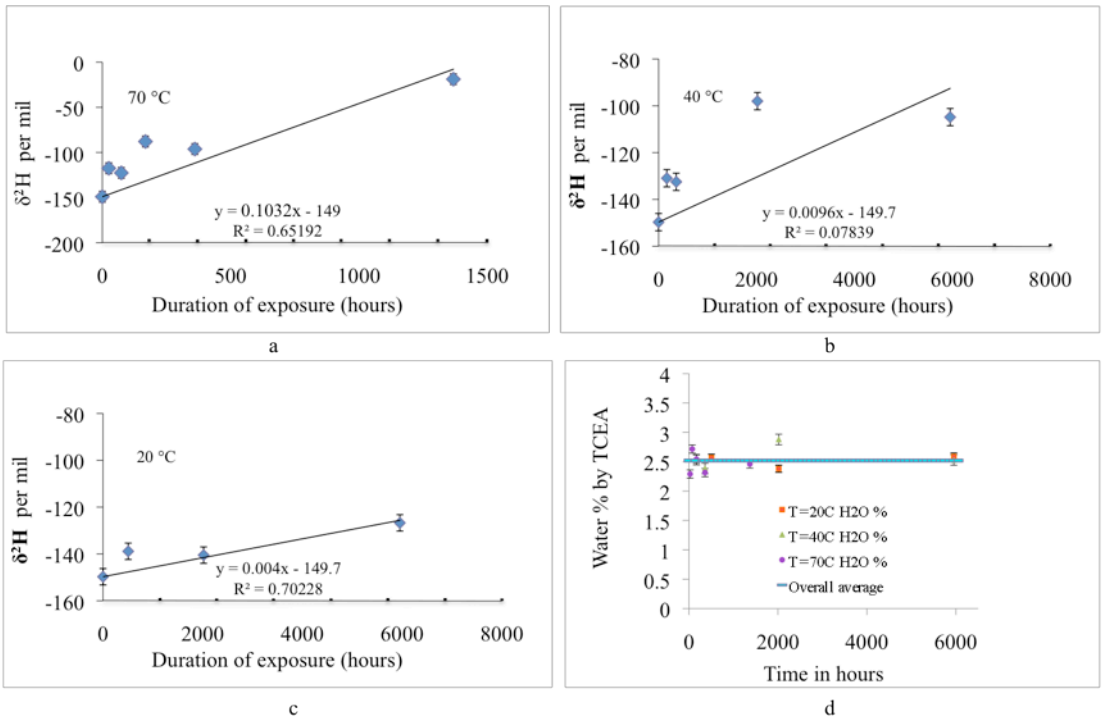

Figure 5

Figure 5 a-d. δ^2H for ash that was first vacuum dried for 60 hours before immersion in the 650 ‰ δ^2H water at a) 70 °C, b) 40 °C, and c) 20 °C. This ash was re-dried for 48 hours post reaction before TCEA analysis. Each data point represents averages of multiple trials with average standard deviations of 6.4 ‰ at 70 °C, 2.5 ‰ at 40 °C, and 3.5 ‰ at 20 °C. Figure 5 d) shows the averages of water contents in the dried material as determined by TCEA, grouped by exposure temperatures, with uncertainties indicated with vertical error bars. Again the length of exposure to isotopically-labeled water does not increase water concentration. Data is summarized in Table 2.

Table 2. Summary of results from TC/EA analysis

Ash zero	N	δ^2H‰ SMOW	σ	wt % H_2O	σ
0 hours exposure	2	-157.7	0.4	2.66	0.02
0 hours exposure	2	-155.0	0.6	2.34	0.00
0 hours exposure	2	-151.6	1.5	2.72	0.02
0 hours exposure	2	-147.3	1.3	2.36	0.01
0 hours exposure	3	-141.3	2.9	2.41	0.08

Native ash reaction series: 70°	N	δ ^{2}H‰ SMOW	σ	wt % H_2O	σ
48 hours immersion	2	-141.4	4.8	2.70	0.04
48 hours immersion	2	-145.9	0.6	2.83	0.07
146 hours immersion	2	-136.7	3.6	2.49	0.09
146 hours immersion	2	-139.8	0.1	2.51	0.01
239 hours immersion	1	-135.3		2.66	
239 hours immersion	2	-142.8	10.1	2.67	0.01
239 hours immersion	2	-139.2	2.6	2.82	0.03
239 hours immersion	2	-138.0	5.9	2.90	0.02
835 hours immersion	2	-129.1	3.4	2.51	0.09
835 hours immersion	2	-130.8	2.4	2.58	0.07
835 hours immersion	2	-114.3	0.9	2.83	0.03
1194 hours immersion	2	-123.2	1.0	2.44	0.01
1194 hours immersion	2	-123.0	3.1	2.48	0.09
1194 hours immersion	2	-117.1	3.1	2.51	0.02
1194 hours immersion	2	-94.6	7.6	2.90	0.02
2838 hours immersion	3	-63.0	2.4	2.86	0.02
3345 hours immersion	3	-42.0	5.9	2.92	0.24
4929 hours immersion	2	10.9	4.5	3.22	0.24
12777 hours immersion	3	67.4	4.5	2.53	0.63
Native ash reaction series: 40°	**N**	**δ ^{2}H‰ SMOW**	**σ**	**wt % H_2O**	**σ**
171 hours immersion	2	-140.1	5.5	2.80	0.04
171 hours immersion	2	-142.6	4.7	2.90	0.00
171 hours immersion	2	-144.8	2.7	3.02	0.03
171 hours immersion	2	-154.7	2.8	3.08	0.10
435 hours immersion	2	-155.6	0.4	2.94	0.21
435 hours immersion	2	-144.5	0.9	2.95	0.10

435 hours immersion	2	-144.2	3.7	2.97	0.04
435 hours immersion	2	-148.8	9.1	3.08	0.22
600 hours immersion	2	-140.6	5.0	2.99	0.06
600 hours immersion	2	-141.6	3.3	3.03	0.03
600 hours immersion	2	-143.6	5.8	3.08	0.04
600 hours immersion	2	-152.7	4.3	3.11	0.05
2450 hours immersion	3	-134.7	4.4	2.54	0.20
2450 hours immersion	3	-137.2	1.7	2.95	0.05
8480 hours immersion	3	-121.3	6.1	2.87	0.20
13952 hours immersion	3	-122.4	1.9	2.59	0.11
Native ash reaction series: 20°	**N**	**δ ^{2}H‰ SMOW**	**σ**	**wt % H_2O**	**σ**
1494 hours immersion	3	-140.9	1.1	2.39	0.03
5064 hours immersion	3	-133.5	4.1	2.63	0.01
8982 hours immersion	3	-143.2	1.3	2.76	0.12
14454 hours immersion	3	-138.4	2.9	2.67	0.04
Pre-dried ash reaction series: 70°	**N**	**δ ^{2}H‰ SMOW**	**σ**	**wt % H_2O**	**σ**
25 hours immersion	3	-117.5	1.4	2.29	0.06
74 hours immersion	2	-121.5	3.2	2.68	0.22
74 hours immersion	3	-122.6	2.1	2.74	0.10
168 hours immersion	3	-87.9	2.8	2.55	0.02
361 hours immersion	3	-96.3	21.2	2.32	0.08
1368 hours immersion	3	-18.9	7.9	2.46	0.03
Pre-dried ash reaction series: 40°	**N**	**δ ^{2}H‰ SMOW**	**σ**	**wt % H_2O**	**σ**
168 hours immersion	3	-130.9	1.0	2.54	0.24
361 hours immersion	3	-132.5	4.0	2.38	0.05
2018 hours immersion	3	-98.0	4.5	2.88	0.03
5954 hours immersion	3	-104.8	0.4	2.53	0.02

Pre-dried ash reaction series: 20°	**N**	**δ ^{2}H‰ SMOW**	**σ**	**wt % H_2O**	**σ**
506 hours immersion	3.0	-138.9	5.9	2.57	0.05
2018 hours immersion	3.0	-140.5	1.2	2.38	0.07
5954 hours immersion	3.0	-126.7	3.5	2.59	0.06
Variable drying time series: no drying	**N**	**δ ^{2}H‰ SMOW**	**σ**	**wt % H_2O**	**σ**
0 hours immersion	2	-140.1	1.0	3.78	0.04
0 hours immersion	2	-137.6	3.9	3.77	0.01
48 hours immersion	2	-119.0	1.9	3.93	0.04
146 hours immersion	2	-97.2	5.5	3.50	0.00
239 hours immersion	2	-103.1	0. 5	3.74	0.00
239 hours immersion	2	-91.4	1.1	3.97	0.08
835 hours immersion	2	-43.2	0.9	3.84	0.01
835 hours immersion	2	-37.3	2.3	3.81	0.04
1194 hours immersion	2	3.3	17.1	4.04	0.04
7353 hours immersion	3	83.2	1.5	3.68	0.01
12777 hours immersion	3	180.1	9.9	4.06	0.04
Variable drying time series: 10 hour	**N**	**δ ^{2}H‰ SMOW**	**σ**	**wt % H_2O**	**σ**
0 hours immersion	3	-144.9	1.0	3.72	0.03
48 hours immersion	3	-127.5	0.3	3.79	0.04
146 hours immersion	3	-104.4	1.0	2.97	0.06
239 hours immersion	3	-106.0	0.2	3.64	0.06
239 hours immersion	3	-95.6	1.3	3.72	0.04
835 hours immersion	3	-48.6	4.4	3.80	0.10
Variable drying time series: 40 hour	**N**	**δ ^{2}H‰ SMOW**	**σ**	**wt % H_2O**	**σ**

0 hours immersion	2	-151.6	1.5	2.72	0.02
48 hours immersion	2	-145.9	0.6	2.83	0.07
146 hours immersion	2	-139.8	0.1	2.51	0.01
239 hours immersion	2	-139.2	2.6	2.82	0.03
239 hours immersion	2	-138.0	5.9	2.90	0.02
835 hours immersion	2	-114.3	0.9	2.83	0.03
1194 hours immersion	2	-94.6	7.6	2.90	0.02
Variable drying time series: 48 hour	**N**	**δ ^{2}H‰ SMOW**	**σ**	**wt % H_2O**	**σ**
1194 hours immersion	2	-123.0	3.1	2.48	0.09
Variable drying time series: 160 hour	**N**	**δ ^{2}H‰ SMOW**	**σ**	**wt % H_2O**	**σ**
835 hours immersion	2	-129.1	3.4	2.51	0.09
1194 hours immersion	2	-123.2	1.0	2.44	0.01
Variable drying time series: 190 hour	**N**	**δ ^{2}H‰ SMOW**	**σ**	**wt % H_2O**	**σ**
0 hours immersion	2	-147.3	1.3	2.36	0.01
48 hours immersion	2	-141.4	4.8	2.70	0.04
146 hours immersion	2	-136.7	3.6	2.49	0.09
239 hours immersion	2	-142.8	10.1	2.67	0.01
239 hours immersion	1	-141.6		2.66	
835 hours immersion	2	-130.8	2.4	2.58	0.07
1194 hours immersion	2	-117.1	3.1	2.51	0.02
Native ash reaction: 40°, no drying	**N**	**δ ^{2}H‰ SMOW**	**σ**	**wt % H_2O**	**σ**
171	2	-136.1	4.0	3.72	0.05
171	2	-134.1	3.2	3.65	0.01

435	2	-127.0	3.5	3.71	0.01
435	2	-116.4	5.4	3.44	0.13
600	2	-126.4	1.3	3.86	0.12
600	2	-124.5	5.5	3.67	0.01

It is important to note that identically-handled samples of native ash that followed our experimental protocol and were: weighed, immersed in water for short or long duration, dried, then washed with solvent (acetone) and dried again by air evaporation of solvent, and re-weighed showed no net uptake of water within the accuracy of this handling procudure and weight determination on microbalance of several microgram. This suggests that the native material while undergoing D/H exchange is not gaining water weight (fig. 6).

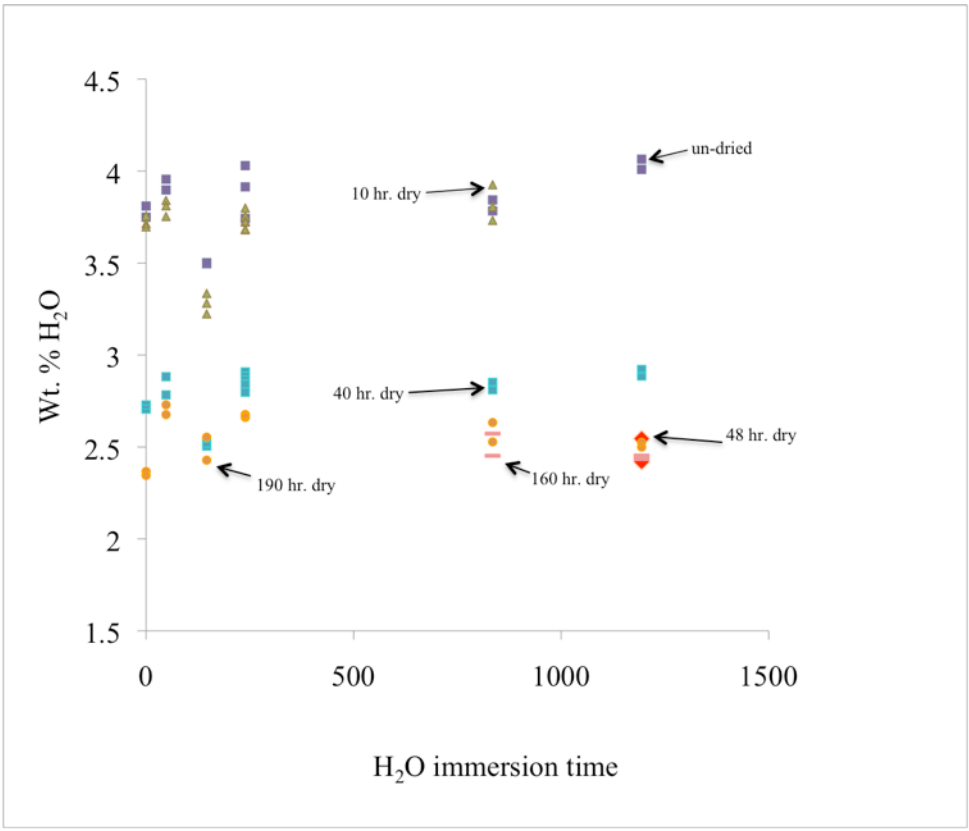

Figure 6

Figure 6. Weight % water in ash vs immersion time in isotopically labeled water and length of subsequent drying at 130 °C for 10 to 190 hours. Samples plotted here demonstrate significant deuterium uptake (Figs. 4-5) but they do not uptake water. Notice that drying for different lengths of time uniformly decreases H_2O concentration from ~3.75 to ~2.5 wt% after which it stops decreasing, starting from 48h. We therefore adopted 48h as a drying time in our runs.

3.3.2. ^{18}O TC/EA mass spectrometry results

The TCEA's CO method was used to measure $^{18}O/^{16}O$ ratio of rapidly released water by thermal decomposition of ash (fig. 7). The $\delta^{18}O$ in ash was compared with a $\delta^{18}O$ water extracted from NBS30 biotite standard that was analyzed concurrently by TCEA in the same analytical session. Given the bulk NBS30 $\delta^{18}O$ value of 5.12‰ from the IAEA reference sheet (nucleus.iaea.org/rpst/Documents/NBS28_NBS30.pdf), and the $\alpha_{(18Osilicate-OH)}$ fractionation, 1.028, for biotite (Zheng 1993) the measured $\delta^{18}O$ of NBS30, rapidly extracted water was corrected to -22.26‰ which is -27.4 ‰ depleted relative to the bulk $\delta^{18}O$ value of NBS30 biotite. The ash value by TCEA corrected to the same NBS30 offset was -23.0 ‰. It can be suspected that there is also a isotope exchange between the rapidly released water and silicate portion of the ash during few seconds of thermal decomposition, but the observations above suggest that these are relatively minor. Nonetheless we are not attributing quantitative values to $\delta^{18}O$ water in ash and use them for relative comparison purpose with the concurently analyzed ash which has been exposed to +56 ‰ water for 7600 h. This is illustrated in figure 7 a,b that despite the rapid increase in $\delta^{2}H$ in exposed ash, this trend is not mirrored in $\delta^{18}O$ numbers. We

conclude that there is no measurable $\delta^{18}O$ exchange in water portion of ash that we can resolve analytically in samples run identically.

3.4. Results of infrared measurements of ash pressed in KBr pellets

The 45% ash/55% KBr mixtures pressed into pellets, were examined by FTIR. The blank run with pure potassium bromide pellet returned no water peaks, and demonstrated low and flat background as is shown in figure 8, in contrast to great diversity observed for pellets with ash, which demonstrate characterisic absorbances in OH and H_2O_{mol} groups.

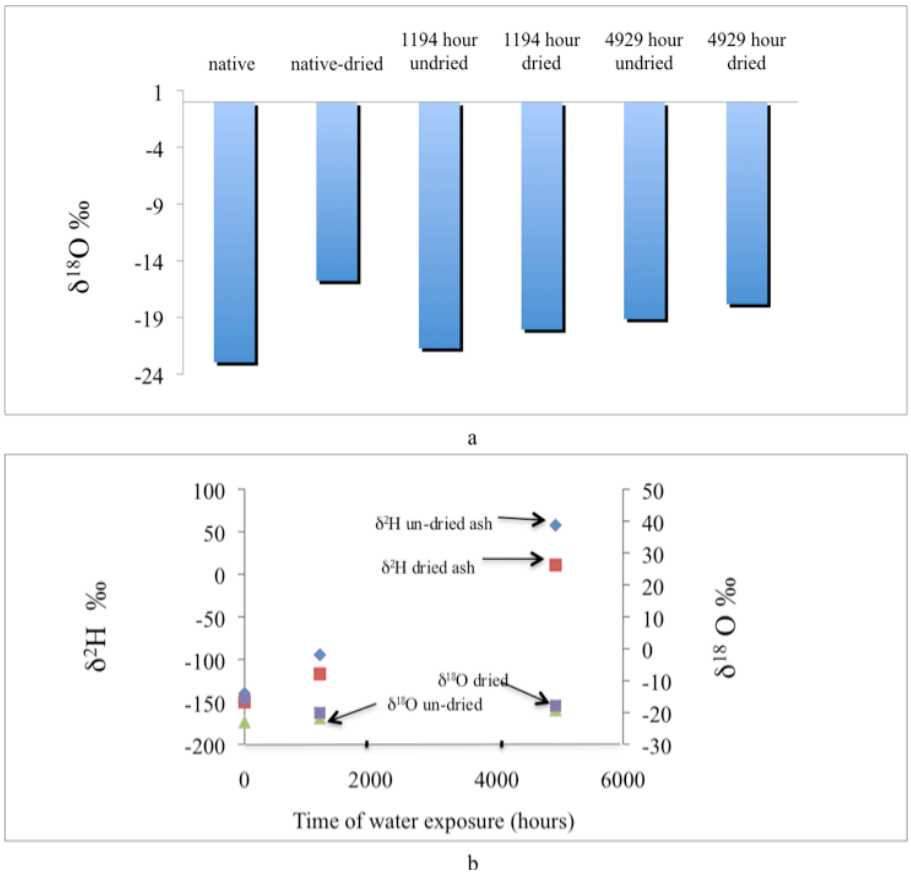

Figure 7

Figure 7 a,b. $\delta^{18}O$ in released water vs immersion time of ash. In (a) the values for $\delta^{18}O$ for native, dried native, and undried and dried reacted ash samples from two immersion times. Values are corrected to hydroxyl oxygen value in NBS30 biotite. Plot b) has comparative $\delta^{2}H$ and $\delta^{18}O$ change in bulk ash as a function of exposure to isotopically-labeled water that demonstrate the effect of deuterium exchange and little to no ^{18}O exchange. The highest amount of enrichment is seen in vacuum drying the native ash. Notice that the scale for hydrogen is about 8 times that for oxygen to normalize for relative mass difference between the heavy and light isotopes in respective H and O systems.

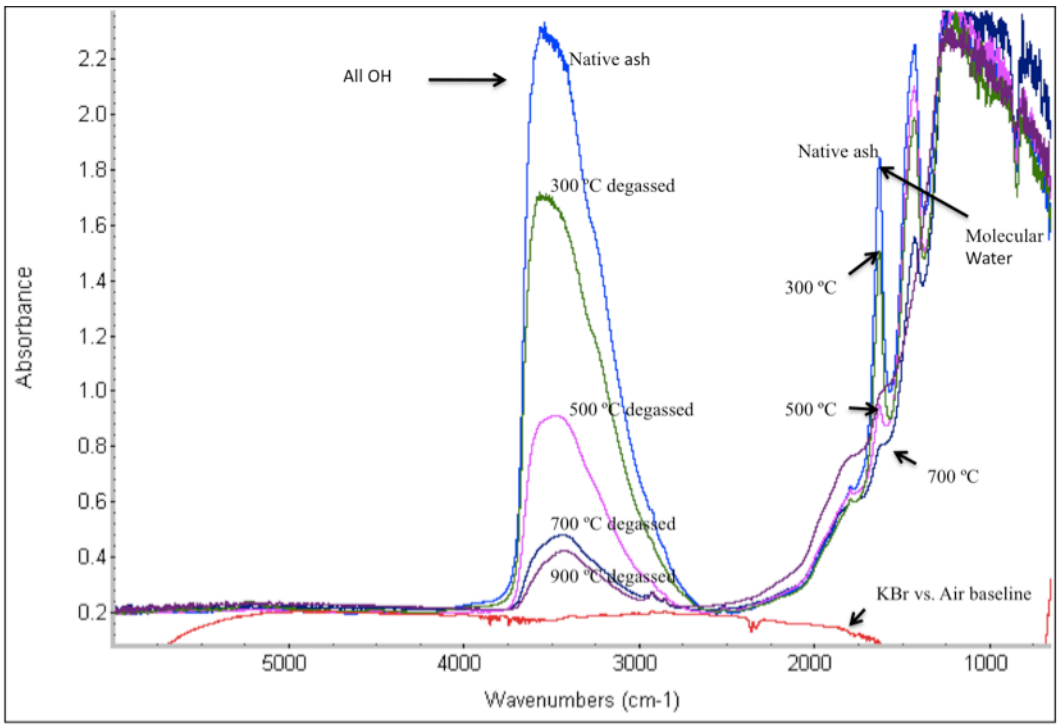

Figure 8

Figure 8. Results of FTIR investigation of water content and speciation step-heated ash sample (actual numbers summarized in Appendix C) that was exposed at 70°C for 7353 hours. The ash was ground and then mixed 55 to 45% with KBr, as described in text. Baseline of KBr versus air shows no water peaks from the salt and unheated samples correspond to the greatest absorbances in both OH and H_2O_{mol} positions. Superimposed IR spectra of successively degassed samples demonstrate progressive decrease in OH and H_2O_{mol} water concentrations (See Fig. 12 below for further discussion of their relative proportions). Notice the signal over baseline for total water plus OH at ~3550 cm^{-1} is easily measurable down to lowest concentrations whereas H_2O only peak at 1640 cm^{-1} decreases to baseline faster.

Next, we are trying to demonstrate water speciation and its changes upon our exposure experiments.

At around 3570 cm^{-1} the absorbance is a composite of SiOH, AlOH, H_2O and possibly other (MOH, M = cation) functional groups. As the absorptivity coefficient ε for our ash in KBr mixtures is not known, but is likely a constant for our identically-prepared mixtures, and we used a published and realistic ε constant of 80 – (1.36 * C_{H2O}) that

gave us good agreement with TCEA results. It is also important to note that sample matrix effects influence ε numbers at all wavelengths and thus there is possibly not a single true value. As noted above we employed the simple formalism of $\varepsilon_{3570} = 80 - (1.36 * C_{H2O})$ (Leschik et al., 2004). Figure 9 demonstrates a linear correlation of IR-determined water concentrations with those determined by TCEA, with nearly zero intercept. It should be noted choice of ε in the range 60-80 does not affect the measure of fit but rather moves the whole set of IR determined water percents up or down.

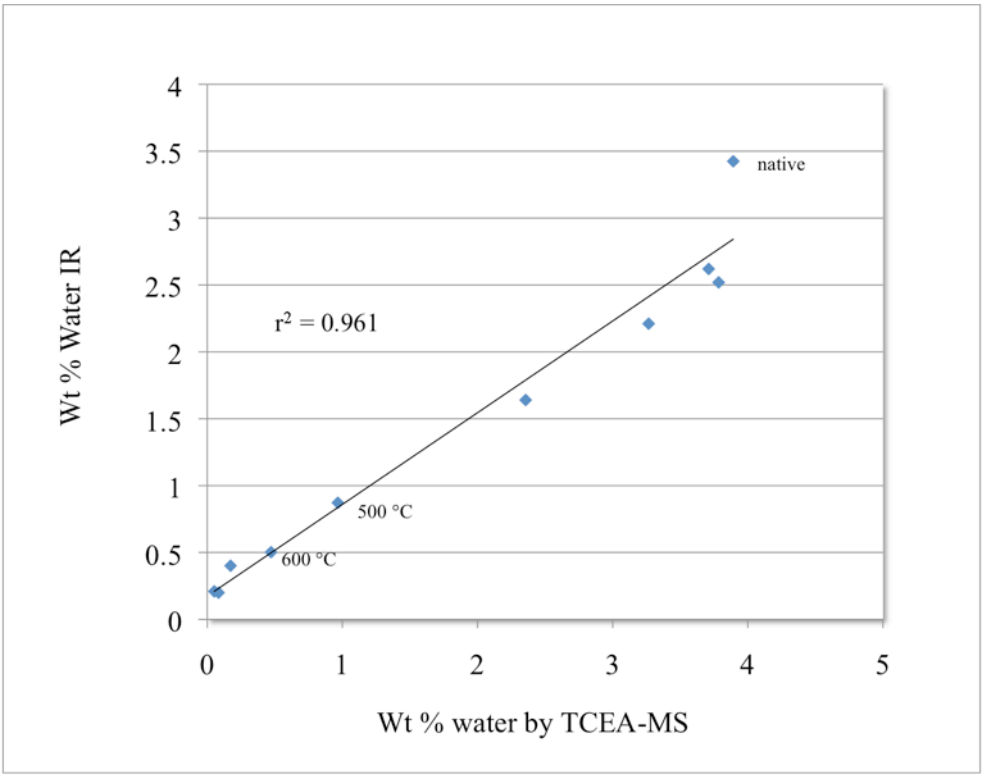

Figure 9

Figure 9. IR vs TCEA water %'s $\varepsilon = 80 - (1.36*C_{H2O})$. Plot of weight percent water determined by the KBr pellet method by IR spectrometry (Figure 8) versus thermal combustion-mass spectroscopy on the same aliquot of samples shown in Figure 8. These were degassed at different temperatures: 100, 200, 300, 400, 500, 600, 700, 800, and 900 degrees in the course of step heating hence the varying water content.

3.5. Step heating experiments

These sets of experiments were run to establish the extent of deuterium substitution at all amounts of remaining water in the ash after variable lengths of vacuum drying.

The results of the step heating experiments are shown in figures 10 a) and 10 b) below. Initially the loss of water and change in deuterium numbers for native ash follow closely what would be predicted from an open system heavy δ^2H water loss as is dictated by the sense of isotope partitioning between remaining OH-richer and δ^2H-poorer ash and δ^2H-richer vapor. At about 1.5-2% water lost these increasingly negative δ^2H values reverse and we attribute this to tapping deeper portion of ash and changing relative proportions of OH/H_2O in the degassed portion. The high to low δ^2H profile for the 7353 hours reacted ash sample is consistent with a picture of in-diffused water or deuterium. What is significant is the deuterium substitution seen at all levels of remaining water.

3.6. TCEA mass spectroscopy, drying and infrared determination

The essential data here are summarized in figures 11 and 12. The ratios of water as SiOH to molecular water or the speciation ratios in 11 correspond closely to other low temperature IR speciation data (Sowerby and Keppler 1999). These latter values in turn are described by and agree with a Langmuir speciation theory (Doremus 2000). In short this notion holds that speciation below the glass transition is determined by total bulk water content and is not affected by temperature below 500-600 °C. Here it is clear that step heating does not reset the speciation values, in agreement with Sowerby (1999). Thus the measured $SiOH/H_2O$ speciation numbersare taken to reflect water in the ash. It is apparent that as drying proceeds, the remaining water in ash is OH-richer, and the

increasing relative amounts of SiOH reflect a fundamental change in the type of water in the ash as "outer" layers are removed by drying. It is apparent from figure 12 that vacuum drying at 130 °C to remove bound molecular water accomplishes this and additionally removes around .3% OH water. The δ^2H values of vacuum dried native ash, about -149 ±5‰, agree well with those in those in the range of 200-500 °C seen in the step heating numbers for native ash (figure 10a). This extended stable range of δ^2H values with regard to water content implies that small variations in the water drying level will not introduce significant error with regard to the δ^2H level. That the δ^2H value of vacuum dried native ash falls within that range confirms a good baseline δ^2H value and the observed small deviations in drying are not major variables affecting this starting point.

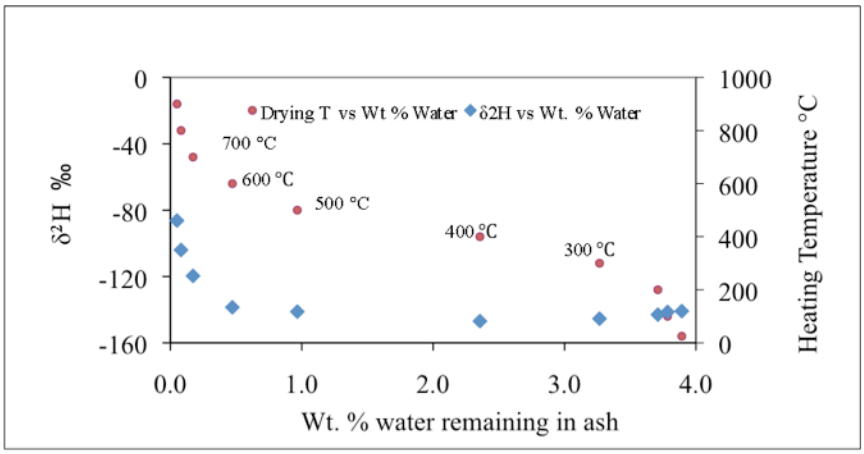

a

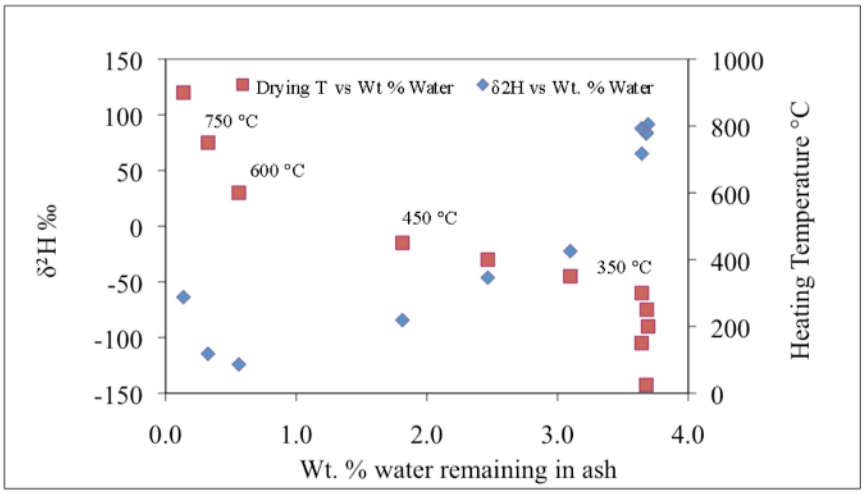

b

Figure 10

Figure 10 a,b. δ^2H vs wt % water by heating temperature for a) native and b) reacted, 7353 hour exposed ash. Scales on the right show drying temperature corresponding to the remaining water. Notice in native ash that although there is a pronounced loss of water, δ^2H does not change dramatically for heating past 300 ºC.

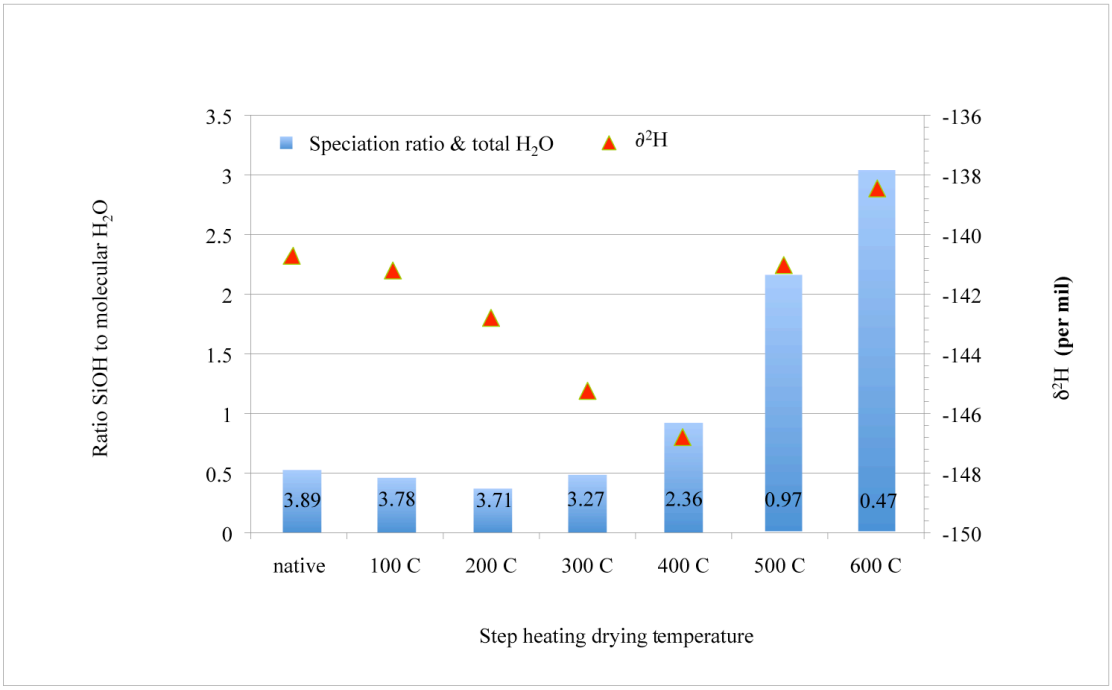

Figure 11

Figure 11. Water speciation during step heating experiment (see fig. 8) with δ^2H overlaid shown. Water percents are from TCEA determinations. Note that H_2O_{mol} and OH are both decreasing but H_2O_{mol} is decreasing a bit faster leading to a slight decrease in δ^2H from native to 400 ºC. There may be some intramolecular deuterium enrichment in $H2O_{mol}$ over the SiOH portion of ash water. The increase in δ^2H from 400 to 600 ºC comes as a result of sampling some apparent δ^2H "reservoir" in the last remaining ash water ending at -86 ‰ δ^2H (fig. 8) which complicates interpretation.

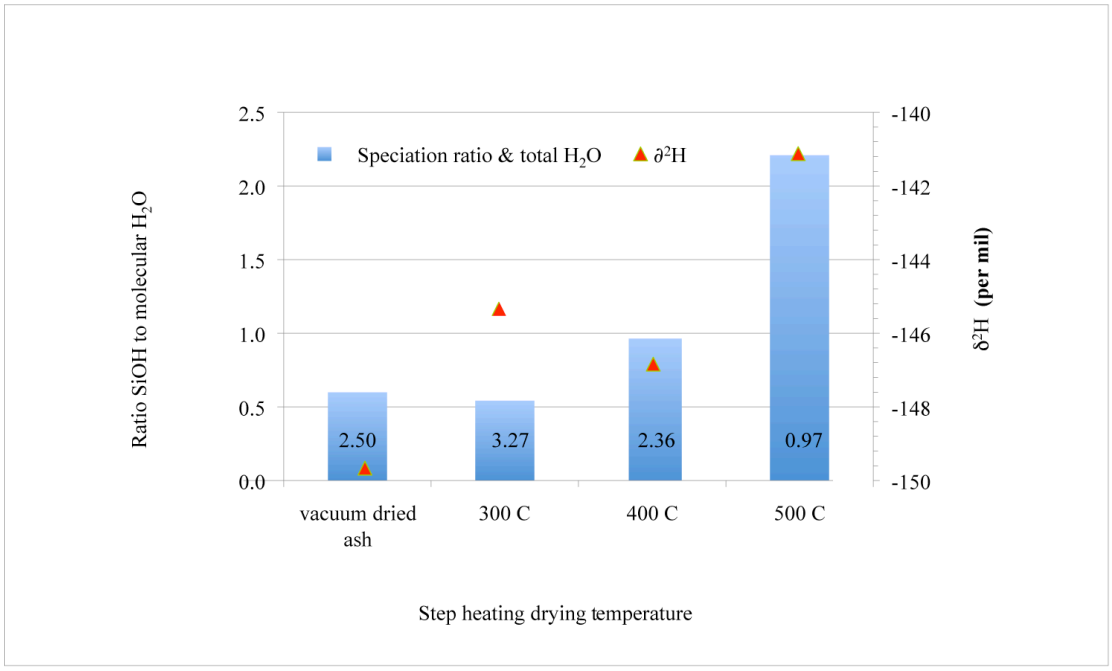

Figure 12

Figure 12. Subset of figure 11 comparing the vacuum dried ash with the 300, 400, and 500 ºC degassed samples. Note there is some loss of SiOH in the vacuum dried but this is accompanied by a greater loss of H_2O_{mol}.

CHAPTER IV

DISCUSSION AND CONCLUSIONS

Co-authored and unpublished material is presented in this chapter. The writing is entirely mine. I. Bindeman provided editorial assistance.

4.1. Summary of observations

1) Loss-on-dry experiments coupled with a comparative TGA analysis between native and dried ash (figure 2) show that a 48 hour period of vacuum drying is sufficient to remove around 1-1.2% of the water in ash. Infrared analysis of ash dried under vacuum at ~130 °C shows dominantly loss of molecular water with measurable hydroxyl loss. Step-heating experiments on native ash show δ^2H of the remaining water in ash stays relatively constant (Fig.10 a) or only slowly decreases until the ash is heated to past 200-220°C.

2) Samples incubated at 70 ˚C with 650 ‰ δ^2H water and dried as outlined above gain approximately 5‰ δ^2H in as little as 48 hours (fig. 4), this representing 0.625% exchanged reaction progress from -145‰ to +590‰ (ash in full equilibrium with +650‰ water). With increasing exposure time at 70 ˚C to 208 days these values simply and linearly increase to over 100 ‰ δ^2H uptake, or 12.5% reaction progress. The δ^2H increase correlates with temperature with proportionately lower increases at 40 and 20 ˚C (fig. 4,5) and demonstrate rapid exchange in surface to lower diagenetic conditions.

3) We also observe a correlation with the intensity of prior vacuum drying and subsequent d^2H uptake: the reacted native ash that has been only solvent rinsed and air dried gives 21% uptake in 1194 hours, 27 % after 4929 hours (70°C, undried ash δ^2H values in fig. 7b). In addition native ash dried at 130°C to less than 3% both before and

after reaction evinces a much higher rate of around 18% after 1400 hours as seen in figure 5.

4) These increasing δ^2H values occur with no net uptake of water (fig. 6), nor any appreciable increase in $\delta^{18}O$ water in ash (fig. 7 above). These results suggest that the deuterium increase is apparently due to proton absorption and exchange and not as a result of water addition or in-diffusion.

5) Our observations are more consistent with "a reactive surface model", the absorption of exchange at the large surface area of the ash plays the most prominent role in exchange. We estimated above that 1 g of Mt Mazama Ash has 0.5±0.1 m^2/g surface area, and figure 13 a. demonstrates how the ash tortuosity leads to a surface area per unit volume increase by a factor of 1.55 relative to a sphere of the same volume.

6) With a relatively rapid surface reaction, the movement of deuterium into the ash is the rate determining step; modeling for a spherical particles (figure 13 b) demonstrates stepwise how glass in outermost microns of large particles, as well as the smallest ash particles in their entirely are rapidly transformed ("consumed") into glass in δ^2H isotopic equilibrium with ambient water. Hypothetical mechanisms of penetration along micro-cracks in the ash are shown in the two stylized ash particles on the right; the furthest right shows water moving along micro-cracks reaching possible remnant bubbles in the ash. Figure 14 demonstrates the volume change for this ash population as a function of diffusion depth. Note how quickly volume is consumed with small changes in-diffusion process or its depth. At 1 micron, a likely deuterium saturation depth, 32% of the total ash volume has been penetrated.

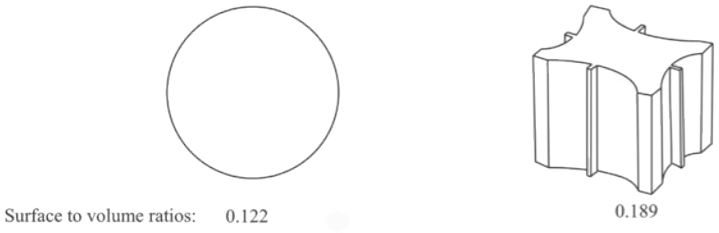

figure a

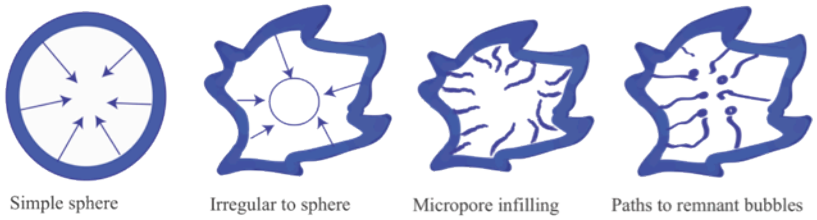

figure b

Figure 13

Figure 13 a,b. Estimating the specific surface area of ash particles based on measured sample size distribution median and SEM photographs (Fig. 3), as compared the sphere of the same volume. First picture depicts the most common ash morphology of Mazama ash prism with ridges. b) diffusion in a spherically symmetric solid (right) is contrasted with Mt Mazama ash. (second from left). Solvent fronts are seen in blue. Note that with time the diffusion front in the random shape becomes more spherical. Two other scenarios are seen on the two right figures. Second from right illustrates permeation through micropores and the far right shows convoluted paths reaching remnant bubbles in interior.

7) Supporting the reactive layer model, our experimentation with a sample immersed in 650 ‰ δ^2H water for over 300 days at 70 °C, degassed and sampled at increasing temperature intervals (Fig. 10 b) demonstrates the loss of initially very high δ^2H water (see Table 3).

This is a representation of a shallow, in-glass water stored in smallest ash particles and the outermost layers of large particles. Increased temperature (fig. 10 b above) of degassing results in the release of progressively less enriched in δ^2H water seen in Table 3. Water remaining in the ash is still enriched up to 20 ‰ δ^2H even at at .10 % water when compared to native ash. This incremental analysis supplements and demonstrates the validity of the cartoon notion on figure 13 (b) showing step-function hydration front on the surface proceeding inward for each of the ash particles. This also supports our conclusions above on the predominance of the surface dynamics, relative to the in-diffusion.

8) We also notice in our experiments that the "surface absorption and reactive potential" of ash is not a constant. Ash that was dried to lower water concentrations before the experiment and then exposed to isotopically-labeled water for equal amount of time, gain greater amounts of deuterium in a similar linear fashion (and not water, nor ^{18}O) as compared to native and not pre-dried ash (fig 5 a-c above). Thus by changing the "surface reactivity" of the ash, removing outer water layers, we illustrate that it is the surface dynamic saturation that plays the most important role.

9) Our longest-duration run at 70°C temperature (12777h, fig. 4 a.) demonstrate that the reaction rate eventually slows down, as the 12777 hour run product does not fall on the same linear trend. We suggest that this observation may signal that all the shallow

sites on the ash were saturated and that the role of a more slow process of deuterium in-diffusion becomes important. Diffusive processes tend to slow down with time as diffusing distance and gradient is increasing, approximately as a square root of time ($x= (Dt)^{1/2}$). Some single point diffusion coefficient estimations can be made by comparing the δ^2H values and their associated, computed depths (see Appendix D) in figure 15 with the times similar δ^2H occur in figures 4 a-c (i.e. the δ^2H value of -119 at 1 micron in figure 15 is close to the 70 ˚C experimental value at 1194 hours in figure 4 a). For the lower temperatures times to δ^2H values can be calculated by projection of the regression equation. These calculated, volume element related δ^2H values are found in Table 8 (Appendix D) and associated with their calculated volume and mass of water amounts.

Table 3. Mass balance calculated deuterium concentrations lost between steps of degassing seen in Figure 10 b. tabulated by increments of water lost. High amounts of deuterium are seen in the first released water. Subsequent released water though enriched shows a rapid decrease in deuterium concentration.

Successive degassed H_2O %	δ^2H of released water
0.55	561
0.63	70
0.65	60
1.25	-67
0.24	-78

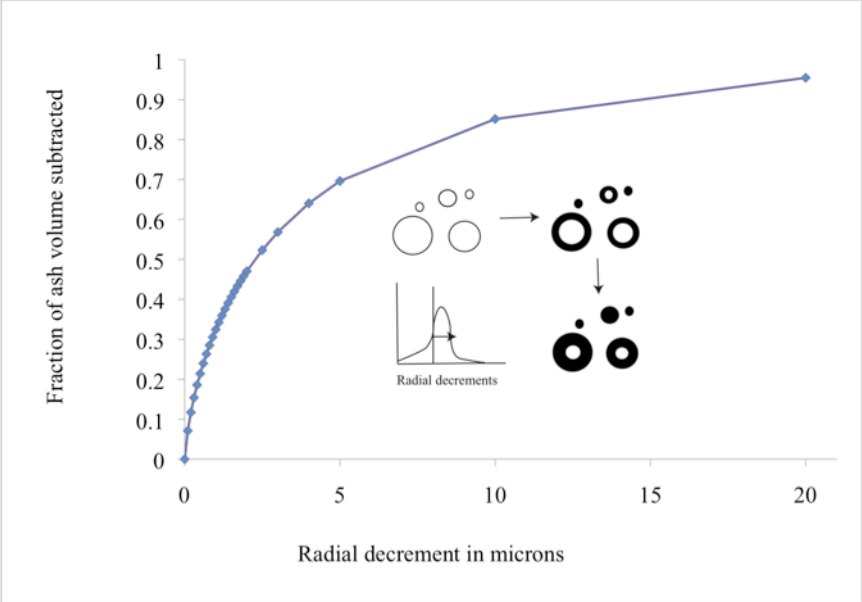

Figure 14

Figure 14. Rapid calculated ash volume decrease results as micron radial increments are subtracted from each particle radius. Sphere sizes are from the data in Figure 1. Spherical approximations to the ash particle population are seen decreasing in the inset.

4.2. Different kinds of water in ash and isotope exchange

Our observation that a surface controlled reaction determines most of exchange and the fact that δ^2H of ash decreases rapidly with drying or degassing suggest that there is an important surface bound water reservoir, which is directly or indirectly hydrogen-bound to a network or backbone of SiOH. This least strongly held water is represented by molecular water bound in a ratio of 2:1 to surface SiOH groups (see fig. 11). This outer network of hydrogen bound water is at once both capable of rapid hydrogen-deuterium exchange at the outermost regions and functions as a potential barrier to further hydrogen or deuterium penetration. The high reactivity that resulted from stripping outer water away before reaction (by drying fig. 5 vs fig. 4) demonstrates how these outer hydrogen

bound waters can function as an impediment to exchange forming essentially the diffusional boundary.

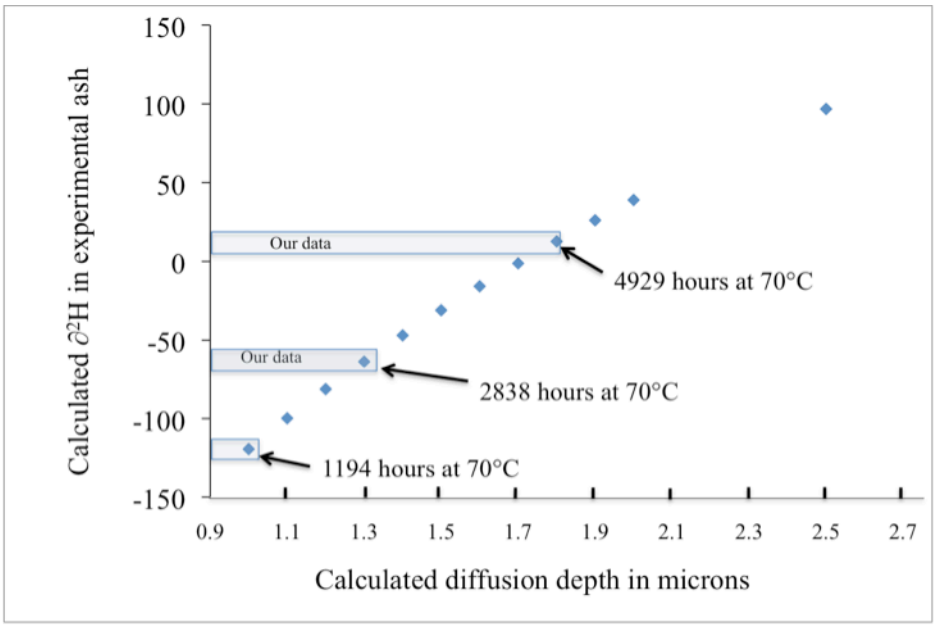

Figure 15

Figure 15. Saturation values of deuterium are summed for each diffusion depth. Abbreviated procedure for calculation is in Table 4 caption and more elaborated in Appendix D.

Given that there are no in situ techniques that would allow us to image spatial distribution of water and SiOH across ash paricles, we rely on semi-quantitative observations of change in their proportion upon degasing (fig. 11). The IR speciation data (fig. 11) of progressively degassed samples demonstrates that this outer 2:1 (molecular to SiOH water) layer gives way to ratios closer to 1:1 at geater progress of the degassing reaction and with lower remaining total water amounts, then go down further past 1:2 water to SiOH. Whether viewed as discrete layers or continuously varying in combining

ratios these speciation ratios are the fundamental chemical underpinnings to the sense of how water exists in ash. As degassing proceeds, the SiOH that remain at increasingly higher temperatures require more and more energy to be removed in accordance with their structural and bonding relationships in the ash. The amount of molecular water that remains even when most of the total water is driven off suggests that last remnants of hydrogen bound molecular water to SiOH is nearly as stable as the OH to Si bonds themselves.

4.3. Simple kinetic explanations of results observed

We observe very simple linear increase in δ^2H. of ash through 7200h duration of experiment (figs. 4 a-c) and then the rates become reduced, which suggest that the rates represent a combination of both surficial chemical exchange, likely initially relatively rapid, and diffusion of hydrogen and/or water, likely a slower process. Below we present a simple mechanistics model of surface reaction-diffusion process in volcanic ash.

Isotopic exchange in the ash/water system can be described by the following expression:

$$d(^2H)/dt = D_{2H}\, d^2(^2H)/dx^2 + D_{H2O}\, d^2\,(^2H_2O)/dx^2 + R_A$$

where the first two terms are Fick's second law diffusion expressions for deuterium and water expressed separately and are in-diffusion fluxes associated with deuterium and water molecules and their corresponding diffusion coefficients in rhyolitic glass, δ^2H and D_{H2O} respectively.

Given our observations above that water in diffusion plays almost no role on timescales involved (and result in no water uptake or changes in ^{18}O), we can drop the second diffusion expression term. Because there is a linear increase in deuterium

concentration through time, we suggest that $R_A >> D_{2H}\, d^2\, (^2H)/dx^2$ initally as is argued above.

On short timescales (10-15% of total exchange), the hydrogen in diffusion rates are slow; and upon integration, the deuterium concentration in bulk ash is simply a linear function of time:

$$^2H = R_A t + {}^2H_{initial}$$

On longer timescales (after 10-15% of exchange) the reaction become mostly diffusion-rate limited. Our observations allows us to estimate both the initial reaction rates and diffusion coefficients (Table 4).

An important point of this analysis is the question of time scales for the process of exchange, and these are summarized in Table 4.

4.4. Recommended ash preparation procedures

Our observations lead to the following guidelines for preparing ash for analysis.

1) No more than 48 hours of vacuum drying at 120 to 130 ° C is necessary to remove extraneous water not part of a deuterium isotope analysis.

2) Solvent drying is a useful part of sample preparation. We recommend acetone as it does not exchange with deuterium, is easy to physically separate from ash, and evaporates readily.

3) The vacuum dried ash is not hygroscopic to any significant extent, and this is different than some clays (smectites in particular). We found that exposing ash to “wet” Eugene lab air for 100 and 6000 h result in ~0.1% and 0.3wt% water increase respectively. Even long-term vacuum-dried ash dumped into water (then solvent, and

rapidly dried in air), absorbs minor water amounts and does not re-hydrate to its original state even. Vacuum-dried ash at 220 °C is distinctly hydrophobic.

Table 4. A summary of deuterium exchange reaction and diffusion outcomes. Procedure summarized in Appendix D for diffusion coefficients. Procedure in short: a) calculate volume elements by subtracting sub micron values from each ash particle diameter and recalculate new total volume (from data in Fig. 1) with volume element equal to original volume minus new volume, etc., b) convert volume element to mass by way of density, c) assuming total water is evenly distributed calculate weight water (convert to moles) for each "layer" from known total water %, d) compute number of sites in each water "layer" necessary to come to equilibrium with labeled water (by moles), and e) sum deuterium values for layer by added layer. These incrementally calculated δ^2H can be compared to times for experimental values of δ^2H. By way of comparison of diffusion coefficients a value of around 8 x 10^{-8} at 75°C is reported for obsidian (Anovitz et al., 2004 in figure 5)

Temperature °C	Rate δ^2H/hr	Estimated diffusion coefficient (μm^2/sec)	Estimated time to 15% reaction (δ^2H from -150 to -39 ‰ in years)	Estimated time for 70% diffusion (years)
70	.0306	$1.86x10^{-7}$	0.40	4.3
40	.0026	$1.59x10^{-8}$	5.23	49.9
20	.0008	$4.83x10^{-9}$	15.84	164

4) Infrared analysis of silica by KBr wafer preparation techniques can yield semi-quantitative water assays for single samples. Multiple samplings are required for more quantitative analysis due to a) sample heterogeneity and b) inherent analytical uncertainties associated with IR Beer's Law techniques and c) KBr matrix issues. Analysis for speciation is more robust as internal normalization of SiOH to H_2O_{mol} tends to cancel errors caused by the factors listed above.

4.5. Implications for paleoclimate studies

Overall it is clear from this work that there is a dynamic relationship between the protons in accessible, hydrous portions of naturally occurring glasses and environmental water.

Results of these experiments put quantitative limits on reliability of δ^2H in ash in paleo-climate studies that are primarily controlled by the isotopic environments and temperatures. We hypothesize that hydrogen-deuterium exchange occurs through surface correlated water in addition to diffusion, with the latter having a rate determining effect. The first process is very rapid (years at 20-40°C of mean annual temperature on the surface). However such hot temperature only exist in desert or equatorial environments. As seasonal changes in δ^2H in water are also expected, we note that the annual cycle at 0 to 20C will not be able to severely affect the δ^2H of the ash. However, a prolonged (see Table 3 for years) exposure to isotopically-distinct water will clearly lead to a alteration of D/H information.

On the other hand oxygen incorporated into glasses during the process of hydration and/or weathering appears to be stable in the presence of later water as we do not observe signs of addional water incorporation into ash nor $\delta^{18}O$ exchange. We suggest studying $\delta^{18}O$ in water portion of ash may be a better approach.

APPENDIX A

TABLE OF EXPERIMENTAL OVERVIEW

Table 5. A capsule view of the experimental design of reacted Mazama ash.

Prior Treatment	Immersion Temperature	Immersion Times (hours)	Goal	Outcome
None	Not applicable	0	Establish ^{2}H concentration in native ash	Baseline of $\partial^{2}H$ (-149 ‰) for all dried native ash runs
None	20 °C	1494 to 14454	Test for temperature dependent ^{2}H uptake in native ash	Temperature dependent ^{2}H uptake observed
None	40 °C	171 to 13952	Test for temperature dependent ^{2}H uptake in native ash	Temperature dependent ^{2}H uptake observed
None	70 °C	48 to 12777	Test for temperature dependent ^{2}H uptake in native ash	Temperature dependent ^{2}H uptake observed
None	70 °C	1194	Test for ^{2}H and ^{18}O uptake in native ash	^{2}H uptake accompanied by little to no ^{18}O uptake
None	70 °C	4929	Test for ^{2}H and ^{18}O uptake in native ash	^{2}H uptake accompanied by little to no ^{18}O uptake

None	Not applicable	0	Establish ^{2}H concentration in successively degassed native ash samples	native ash degassing $\partial^{2}H$ baseline set
None	70 °C	7017	SEM comparison with native ash ash samples	Samples visually indistinguishable
None	70 °C	7353	Examine ^{2}H uptake in successively degassed ash samples	Decreasing, finite ^{2}H permeation of all OH left in ash
Vacuum dry 125 °C 60 hours	20 °C	506 to 5954	Examine effect of "outer" water removal on temperature dependent kinetics of ^{2}H uptake	Rapid ^{2}H uptake kinetics observed
Vacuum dry 125 °C 60 hours	40 °C	168 to 5954	Examine effect of "outer" water removal on temperature dependent kinetics of ^{2}H uptake	Rapid ^{2}H uptake kinetics observed
Vacuum dry 125 °C 60 hours	70 °C	25 to 1368	Examine effect of "outer" water removal on temperature dependent kinetics of ^{2}H uptake	Rapid ^{2}H uptake kinetics observed

APPENDIX B

IR PROCEDURE AND DATA

All infrared samples were run on a liquid nitrogen cooled detector, Thermo Nicolet NEXUS 670 FTIR spectrometer coupled to a Nicolet Continuμm Infrared Microscope (model no. 912A0429). The number of acquisitions was always 512 and background correction was simply the sodium chloride plate (that the pellets were rested upon) and air. The spectra were recorded in absorbance mode and baseline corrections were made using the Nicolet software to fit the usually sloping baseline beneath the peak. Concentrations were calculated from absorbances using the formula below (Leschik et al., 2004).

$$C_{H2Ot} = M_{H2O} A_{3570}/\rho d\varepsilon_{3570}$$

where M_{H2O} is 18 the molecular weight of water, A_{3570} the total water absorbance centered around this frequency in cm^{-1}, ρ is the density of the glass, d the path length, and ε_{3570} is the Beer's Law extinction coefficient or absorptivity in appropriate units ($lmol^{-1}cm^{-1}$) such that C_{H2Ot} comes out in weight fraction. A similar expression is used for the molecular water absorbance only that exists at around 1640 cm^{-1} and possesses a separate unique ε_{1640}:

$$C_{H2Om} = M_{H2O} A_{1640}/\rho d\varepsilon_{1640}$$

Subtracting C_{H2Om} from C_{H2Ot} affords a reckoning of both molecular water and SiOH as water. For the isotopically shifted OD absorbance the same expression exists for the peak at around 2650 cm^{-1} likewise with its own ε_{2550}. Infrared analysis of water in glass in

effect treats the glass as solvent and as such requires a density correction. Wafers were constructed and difference weighed, die alone and die with pellet.. Thickness was determined as above with a digital micrometer again while the sample was in the die. This exercise yielded a value of 2.2 g/cm^3.

The value of ε is not constant with water weight (Leschik et al., 2004) and these authors formulated an expression for ε in terms of water concentration especially pertinent to values of water greater than 2 wt%:

$\varepsilon_{3570} = 80\text{-}(1 \cdot 36)(C_{H2Ot})$

This works best as an iterative procedure by assuming some initial ε and calculating provisional C_{H2Ot} . Concentrations were initially determined employing an ε value of 74 which falls in the range described in two separate IR studies of 60 (Yokoyama et al., 2008) and 80 (Leschik et al., 2004). These trial C_{H2Ot} values were substituted into the ε_{3570} expression and new C_{H2Ot} values determined, etc. The process converges rapidly. Molecular water ε value of 55 was from an earlier paper (Newman et al., 1986).

Initial preparations were done to optimize the ash to KBr ratio, which turned out to be about 45 % ash / 55% KBr. The mixture determination was done in concert with determining a total mixture amount that could be easily handled once pressed into a wafer and as a second criterion passes sufficient infrared radiation to be useful. Samples were weighed to a total of about 200 mg. Table B1 summarizes the IR data.

Table 6. Summary of IR data.

1st Step Heat:Temp	**A_{3500}**	**A_{1647}**	**thickness (cm)**	**% ash**	**IR H_2O**	**Speciation ratio**
25	2.085	0.94	0.0149	0.4433	3.42	0.62
100	1.285	0.605	0.0129	0.4225	2.52	0.53
200	1.76	0.884	0.0168	0.4279	2.62	0.43
300	1.511	0.7	0.0161	0.451	2.21	0.54
400	1.212	0.434	0.0171	0.4545	1.64	0.97
500	0.708	0.154	0.0184	0.4581	0.87	2.21
600	0.282	0.048	0.0127	0.4559	0.50	3.07
700	0.274	0.055	0.0151	0.466	0.40	2.45
800	0.148	0.038	0.0166	0.4579	0.20	1.32
900	0.195	0.052	0.0227	0.421	0.21	1.59
2nd Step Heat:Temp	**A_{3500}**	**A_{1647}**	**thickness (cm)**	**% ash**	**IR H_2O**	**Speciation ratio**
25	1.563	0.777	0.0183	0.4256	2.13	0.44
150	1.71	0.78	0.0171	0.4515	2.36	0.40
200	1.68	0.782	0.0154	0.4476	2.61	0.72
250.1	2.19	0.962	0.0211	0.4466	2.48	0.65
250.2	2.008	0.958	0.0188	0.452	2.52	0.51
300	1.815	0.853	0.0185	0.4471	2.34	0.52
350	1.466	0.568	0.0169	0.441	2.08	0.84

400.1	1.32	0.497	0.0228	0.4465	1.36	0.87
400.2	1.327	0.498	0.0228	0.4465	1.36	0.88
450	1.14	0.309	0.0182	0.4572	1.44	1.60
600.1	0.545	0.106	0.0178	0.451	0.70	2.58
600.2	0.558	0.098	0.0191	0.452	0.67	2.96
600.3	0.524	0.092	0.0191	0.452	0.63	2.96
750	0.356	0.069	0.0233	0.45	0.35	2.57
900	0.28	0.067	0.0187	0.4752	0.32	1.89
Vacuum Dried native ash	**A_{3500}**	**A_{1647}**	**thickness (cm)**	**% ash**	**IR H_2O**	**Speciation ratio**
130 C	1.651	0.682	0.0187	0.4537	2.06	0.73
130 C	1.866	0.805	0.0187	0.4537	2.34	0.66
130 C	1.246	0.534	0.0188	0.4515	1.54	0.65
130 C	1.385	0.638	0.0188	0.4515	1.72	0.54
130 C	1.368	0.589	0.0188	0.4515	1.70	0.64

APPENDIX C

TABLE OF STEP HEATING PROCEDURE AND DATA

Table 7. Summary of step heating sequences.

Step heating 1: native ash sampling temperature	**N**	**δ ^{2}H‰ SMOW**	**σ**	**wt % H_2O**	**σ**
25	3	-140.9	3.6	3.89	0.07
100	3	-141.4	2.4	3.78	0.04
200	3	-143.0	0.9	3.71	0.04
300	3	-145.4	1.6	3.27	0.08
400	3	-146.9	0.8	2.36	0.02
500	3	-141.2	1.3	0.97	0.03
600	3	-138.6	1.5	0.47	0.01
700	3	-119.6	5.5	0.17	0.01
800	5	-104.0	4.5	0.08	0.01
900	4	-86.3	14.0	0.05	0.00
Step heating 2: native ash sampling temperature	**N**	**δ ^{2}H‰ SMOW**	**σ**	**wt % H_2O**	**σ**
25	2	-140.8	0.4	3.61	0.12
150	2	-142.2	3.0	3.69	0.07
200	2	-144.0	0.4	3.53	0.33
250	2	-144.8	1.2	3.63	0.00
300	3	-144.7	1.5	3.46	0.03

350	3	-148.3	1.2	2.45	0.13
400	3	-149.2	2.1	2.26	0.08
450	3	-151.6	2.6	1.50	0.01
600	3	-146.1	2.2	0.49	0.01
750	2	-119.4	10.8	0.12	0.01
900	2	-84.2	0.5	0.07	0.00
Step heating 2: reacted ash sampling temperature	**N**	**δ ^{2}H‰ SMOW**	**σ**	**wt % H_2O**	**σ**
25	3	83.2	1.5	3.68	0.01
150	3	87.7	2.7	3.64	0.08
200	3	91.5	2.1	3.69	0.07
250	3	83.8	1.3	3.68	0.10
300	3	65.2	4.0	3.64	0.05
350	3	-22.4	9.7	3.10	0.29
400	3	-46.2	1.7	2.47	0.04
450	3	-84.4	4.3	1.81	0.11
600	3	-124.1	2.4	0.56	0.02
750	2	-114.6	4.0	0.32	0.04
900	1	-63.7		0.14	

APPENDIX D

ESTIMATION OF DIFFUSION AND VOLUME ANALYSIS

The specific surface area (surface to volume ratio) of this ash, calculated from the data presented in figure 1, is 1.065 microns^{-1}. With appropriate unit conversions and using a density of 2.2 g/cm^3 this works out to about .5 m^2/g. This is about 25-50% of typical ash surface area measured by high-resolution nitrogen adsorption/desorption experiments (Delmelle et al., 2005), is a spherical approximation and takes no account of porosity. It is perhaps of significance to note here that these authors (Delmelle et al., 2005) indicate the surface area sampled by water is greater than by nitrogen. As spheres possess the lowest possible surface to volume ratio it is easy to increase specific surface area with simple changes in particle geometry (figure 13 a).

Table 8. Volume-mass analysis table

Diffusion Depth	Fraction volume consumed	g ash	Moles H_2O/layer	g H_2O/layer	Reactive sites/layer	Cumulative ∂^2H by layer	Cumulative ∂^2H by layer-dried ash
0	0.000	2.20	0	0	0	0	0
0.1	0.071	2.04	0.000331	0.00383	3.79E-08	-88	0
0.2	0.117	1.94	0.000213	0.00309	2.44E-08	-54	0
0.3	0.154	1.86	0.000172	0.00266	1.96E-08	-27	0
0.4	0.186	1.79	0.000148	0.00236	1.69E-08	-3	0
0.5	0.214	1.73	0.000131	0.00214	1.50E-08	17	0

0.6	0.240	1.67	0.000119	0.00197	1.36E-08	36	0
0.7	0.263	1.62	0.000109	0.00182	1.25E-08	53	0
0.8	0.285	1.57	0.000101	0.00170	1.16E-08	69	0
0.9	0.305	1.53	0.000095	0.00160	1.08E-08	84	0
1	0.325	1.49	0.000089	0.00151	1.02E-08	99	-129
1.1	0.343	1.45	0.000084	0.00142	9.57E-09	112	-110
1.2	0.360	1.41	0.000079	0.00135	9.06E-09	124	-91
1.3	0.376	1.37	0.000075	0.00129	8.59E-09	136	-74
1.4	0.391	1.34	0.000071	0.00123	8.18E-09	147	-57
1.5	0.406	1.31	0.000068	0.00117	7.80E-09	158	-41
1.6	0.420	1.28	0.000065	0.00112	7.45E-09	169	-26
1.7	0.433	1.25	0.000062	0.00107	7.13E-09	178	-11
1.8	0.446	1.22	0.000060	0.00103	6.83E-09	188	3
1.9	0.458	1.19	0.000057	0.00099	6.56E-09	197	16
2	0.470	1.17	0.000055	0.00444	6.31E-09	206	29
2.5	0.523	1.05	0.000247	0.00375	2.83E-08	245	87
3	0.568	0.95	0.000209	0.00603	2.39E-08	278	136
4	0.640	0.79	0.000335	0.00465	3.84E-08	331	214
5	0.696	0.67	0.000259	0.01299	2.96E-08	372	275
10	0.852	0.33	0.000722	0.00863	8.26E-08	486	443
20	0.955	0.10	0.000479	0.00379	5.49E-08	562	556

Using the data in Figure 14 and Table D1 above and by assuming: 1) an ash density and 2) pre-existing water in the ash is homogeneously distributed throughout the volume it is possible to calculate the number of reactive sites in the ash and hence the saturation

values for deuterium as the ash is permeated. These values are summarized in the table D1 above. The δ^2H values as a running total as diffusion progresses are shown as a function of remaining volume (figure D1) and diffusion depth (figure D2). Vacuum drying removes all the water and support for deuterium values down to about 2.5%. This effectively resets the running totals.

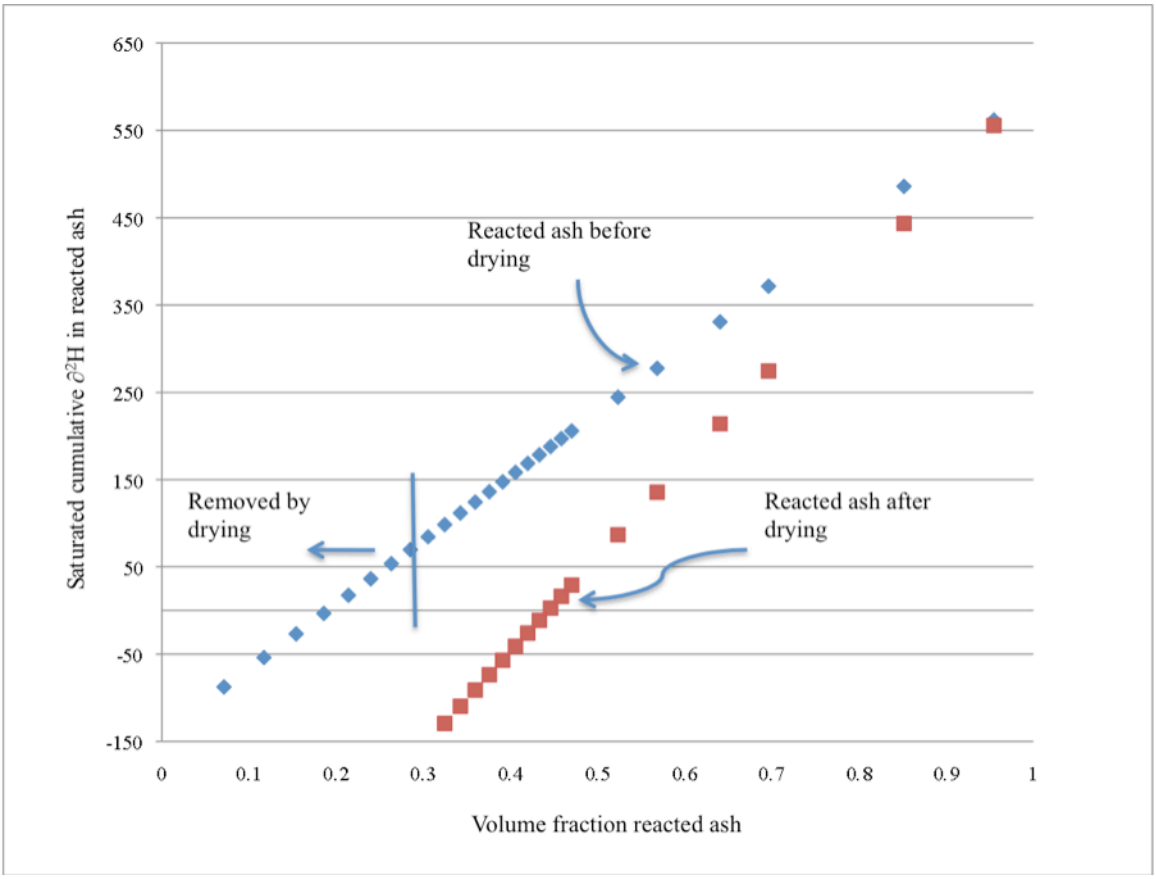

Figure D1. The cumulative δ^2H is seen as each successive volume interval is saturated with deuterium.

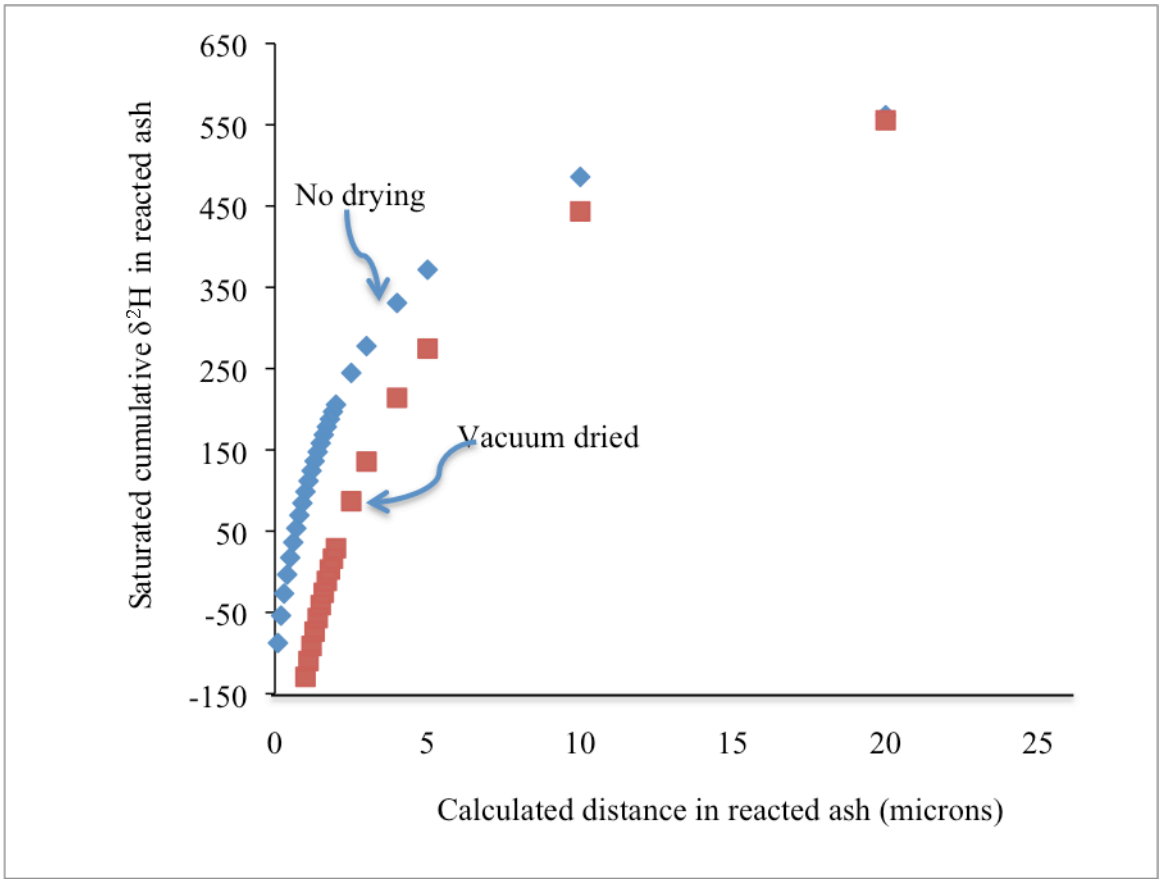

Figure D2. The plot here is essentially the same as B1 but analysis is in terms of radial distance.

These discrete diffusion boundaries are artificial in the sense that a diffusion profile species distribution "tail" may well have penetrated to some further depth beyond some discrete boundary. At this point the water and deuterium tail can well be below the stoichiometric amount necessary to react with all the available ash sites in this layer. That is it is well below saturation. On the other hand the total mass of sites reacted in these limited reaction volumes can be lumped or summed as a total of sites that would be found within some prior volumes of ash. That is if only 10 % of sites are reacted in a newly in diffused front these can be subtracted from the new "layer" and added back to a prior

nearly fully reacted “layer” and so on. These somewhat artificially saturated layers then can be seen as an effective diffusion distance. Finally looking at a set of reasonable diffusion depths for the dried ash, depths from the drying depth of one micron to around 2.5 microns, it is possible to calculate estimations for the δ^2H values with respect to this effective diffusion depth. Each increment of volume (and/or depth) carries some potential for total deuterium saturation. Adding volume element by volume element each containing an accompanying deuterium amount gives a running total with depth. The sum reveals a reasonable inference that can be made about the extent of deuterium penetration with depth or diffusion. These calculated values are directly compared to experimental values in the reacted and dried ash numbers. This is seen in figure 15.

REFERENCES CITED

Anovitz, L M, Cole, D R & Fayek, M. (2008). Mechanisms of rhyolitic glass hydration below the glass transition. *American Mineralogist*, **93**(7), 1166–1178.

Anovitz L., Elam J. M., Riciputi L. R., and Cole D. R. (2004) Isothermal Time-Series Determination of the Rate of Diffusion of Water in Pachuca Obsidian*. *Archaeometry*, **46**(2), 301–326.

Anovitz L. M., Cole D. R. and Riciputi L.R. (2009a) Low-temperature isotopic exchange in obsidian: Implications for diffusive mechanisms. *Geochimica et Cosmochimica Acta*, **73**(13), 3795–3806.

Anovitz L. M., Cole D. R., and Riciputi, L.R. (2009b) Low-temperature isotopic exchange in obsidian: Implications for diffusive mechanisms. *Geochimica et Cosmochimica Acta*, **73**(13), 3795–3806.

Bao H., Koch P.L. and Thiemens M. (2000) Oxygen isotopic composition of ferric oxides from recent soil, hydrologic, and marine environments. *Geochimica et Cosmochimica Acta*, 64, 2221-2231.

Bartholomew R. and Butler B. (1980) Infrared Spectra of a Water‐Containing Glass. *Journal of the American Ceramic Society* **63**(9-10) 481-485

Chamberlain C. and Poage M. (2000) Reconstructing the paleotopography of mountain belts from the isotopic composition of authigenic minerals. *Geology*, **28**(2), 115-118

Dansgaard W. (1964) Stable isotopes in precipitation. *Tellus*, **16**(4), 436–468.

Doremus R. (2000) Water speciation in silicate glasses and melts: Langmuir limited site model. *American Mineralogist*. **85** 1674–1680

Friedman I., Gleason J. and Wilcox R. (1992) Modeling of ancient climate from deuterium content of water in volcanic glass. *Quaternary International*. **13-14** 201-203

Friedman I., Gleason J. and Warden A. (1993) Ancient climate from deuterium content of water in volcanic glass Friedman et al., *American Geophysical Union Monograph*, 78 (Climate Change in Continental Isotopic Records (ed. P.K. Swart, Lohmann, K.C., McKenzie, J., Savin, S.), pp. 309–319.

Friedman I., Izett G.A. and Gleason J.D. (1985) Isotopic paleoclimate from hydrated volcanic ash. *Geol. Soc. Am., Abstr. Programs; (United States)*, **17**.

Gat J.R. (2010) *Isotope Hydrology: A Study of the Water Cycle*, Imperial College Press. 188pp

Kirkland J. (1955) Quantitative application of potassium bromide disk technique in infrared spectroscopy. *Analytical Chemistry*. **27** (10) 1537-1541

Leschik M., Heide G., Frischat G.H., Behrens H., Wiedenbeck M., Wagner N., Heide K., Geiszler H. and Reinholz U. (2004) Determination of H2O and D2O contents in rhyolitic glasses. *Physics and Chemistry of Glasses-European Journal of Glass Science and Technology Part B*, **45**(4), 238–251.

Métrich N. and Wallace P.J. (2008) Volatile Abundances in Basaltic Magmas and Their Degassing Paths Tracked by Melt Inclusions. *Reviews in Mineralogy and Geochemistry* **69**, 363-402

Mulch A. (2006) Hydrogen Isotopes in Eocene River Gravels and Paleoelevation of the Sierra Nevada. *Science*, **313**(5783), 87–89.

Newman S., Stolper E. and Epstein S. (1986) Measurement of water in rhyolitic glasses: calibration of an infrared spectroscopic technique. *Am. Mineral.;(United States)*, **71**, 1527–1541.

Riciputi L. (2002) Obsidian Diffusion Dating by Secondary Ion Mass Spectrometry: A Test using Results from Mound 65, Chalco, Mexico. *Journal of Archaeological Science*, **29**(10), 1055–1075.

Romo L. (1956) The exchange of hydrogen by deuterium in hydroxyls of kaolinite. *The Journal of Physical Chemistry*, **60**(7), 987–989.

Rowley D., Pierrehumbert R. and Currie B. (2001) A new approach to stable isotope-based paleoaltimetry: implications for paleoaltimetry and paleohypsometry of the High Himalaya since the Late Miocene. *Earth and Planetary Science Letters*, **188**(1-2), 253–268.

Sarna-Wojcicki A.M., Shipley S., Waitt R.B., Dzurisin D. and Wood S. (1981) Areal Distribution, Thickness, Mass, Volume, and Grain Size of Air-fall Ash from the Six Major Eruptions of 1980. USGS. In: Lipman, P.W., and Mullineaux, D.R., (eds.), *The 1980 Eruptions of Mount St. Helens*, Washington: U.S. Geological Survey Professional Paper 1250 pp. 577-578

Sobkowiak M. (1995) A comparison of drift and KBr pellet methodologies for the quantitative analysis of functional groups in coal by infrared spectroscopy. *Energy & Fuels*. **9** 359-363

Sowerby J. and Keppler H. (1999) Water speciation in rhyolitic melt determined by in-situ infrared spectroscopy. *American Mineralogist*. **84**, 1843–1849

Wakabayashi H. (1989) Diffusion of water into silica glass at low temperature. *Journal of the American Ceramic Society* **72** (10) 1850-1855

Zheng Y.F. (1993) Calculation of oxygen isotope fractionation in hydroxyl-bearing silicates. *Earth and Planetary Science Letters*, **120**(3-4), 247–263.